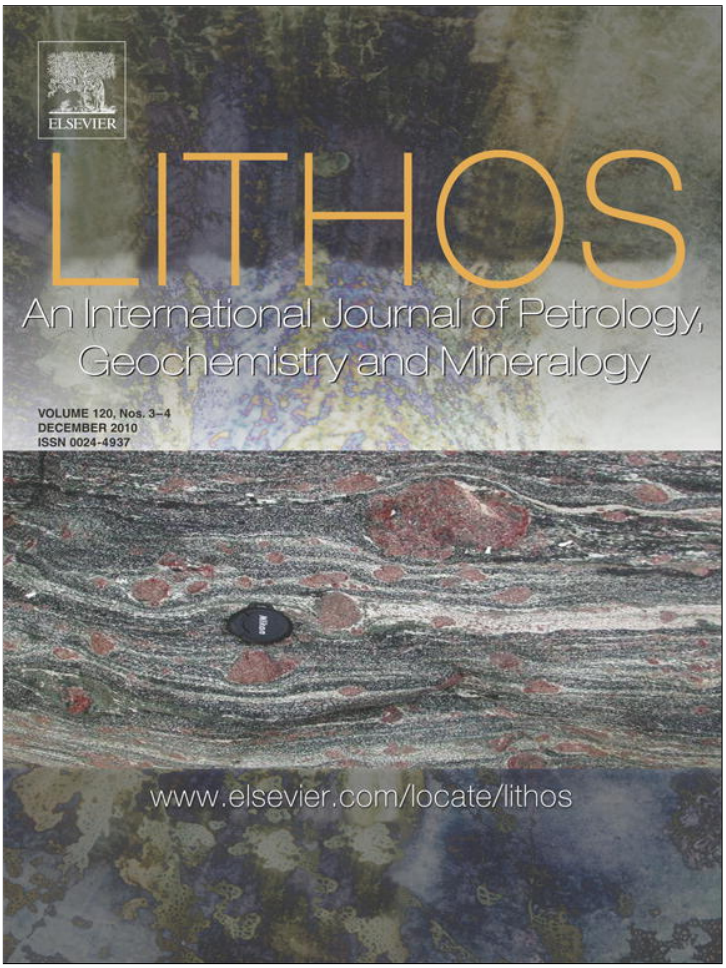

Lithos 120 (2010) 453–474

Contents lists available at ScienceDirect

Lithos

journal homepage: www.elsevier.com/locate/lithos

Initial water budget: The key to detaching large volumes of eclogitized oceanic crust along the subduction channel?

S. Angiboust *, P. Agard

UPMC Univ Paris 06, ISTEP, F-75005, Paris, France
CNRS, UMR 7193, ISTEP, F-75005, Paris, France

ARTICLE INFO

Article history:
Received 15 April 2010
Accepted 14 September 2010
Available online 22 September 2010

Keywords:
Eclogites
Zermatt–Saas ophiolite
Subduction
Exhumation
Lawsonite
Thermodynamic modelling

ABSTRACT

We herein investigate the extent to which extensive hydration of the oceanic lithosphere influences the preservation and exhumation of large-scale ophiolite bodies from subduction zones. The Zermatt–Saas ophiolite (ZS, W. Alps), which was subducted during the late stages of oceanic subduction, preserves a complete section of Mesozoic Tethys oceanic lithosphere and particularly fresh eclogites, and represents, so far, the largest and deepest known portion of exhumed oceanic lithosphere. Pervasive hydrothermal processes and seafloor alteration led to the incorporation of large amounts of fluid bound in the hydrated upper layers of the oceanic crust (now as lawsonite eclogites, glaucophanites, and chloritoschists) and in associated ultramafic rocks.

Internally, the ZS ophiolite is made up of a series of tectonic slices of oceanic crust (150–300 m thick) which are systematically separated by a 5 to 100 m thick layer of serpentinite. This stack of slices is separated from the underlying eclogitized continental crust (e.g., Monte Rosa) by a thick (~500 m) serpentinite sole. Field observations, textural relationships and pseudosection modelling reveal that lawsonite was abundant and widespread in mafic eclogites when the ophiolite detached from the slab at around 550 °C and 24 kbar.

Comparison between fresh eclogitic samples and pseudosection modelling shows that (i) water remained in excess from burial to eclogitic peak conditions, (ii) the lightest eclogitized metabasalts correspond to the portions of oceanic crust where metasomatism was the strongest, (iii) crystallization of widespread hydrated parageneses (such as lawsonite, glaucophane and phengite) instead of garnet and omphacite decreased by 5 to 10% the rock density and subsequently enhanced its buoyancy.

We propose that this density decrease acted as a 'float' which prevented the slices from an irreversible sinking in the mantle. These slices were subsequently detached from the downgoing slab and stacked in the serpentinized subduction channel at pressures between 15 and 20 kbar, in the epidote blueschist facies. Exhumation of the underlying, positively buoyant continental crust dragged this "frozen" nappe-stack from the subduction channel towards the surface.

1. Introduction

Subduction zones are crucial areas for understanding lithospheric-scale coupling between plates, risk assessment, or studying vertical movements and material recycling on Earth. Key petrological proxies, such as blueschists and eclogites (and even more so lawsonite-bearing mafic eclogites) provide important anchor points for thermal models of subduction zones, but also for water recycling into the mantle and arc magmatism (Poli and Schmidt, 1995; Okamoto and Maruyama, 1999; Liou et al., 2000; Forneris and Holloway, 2004; Fig. 1a,b). Pass the accretionary wedge, the mafic oceanic crust is indeed the main sink for water as it contains as much as ~90% of the bound subducted water (Ito et al., 1983; Peacock, 1990) in hydrated phases such as glaucophane, phengite and lawsonite (2.5, 4 and 12 wt.% H_2O respectively).

Most authors, following England and Holland (1979) and Shreve and Cloos (1986), envision the plate–slab interface as a subduction channel in which material may move partly independently from the upper and lower plates. In detail, however, the nature and structure of the subduction channel are still poorly constrained (Raimbourg et al., 2007; Hilairet et al., 2009; Monié and Agard, 2009 and references therein). Recent high-resolution reflexion and tomographic imaging of subduction planes suggest the existence of low-velocity layers, 2–8 km thick, located on top of the slab on several subduction zones (Fig. 1a; Bostock et al., 2002; Abers et al., 2006; Audet et al., 2009), interpreted as sediments, serpentinites, highly hydrated crustal material or slivers lying along the plate–slab interface. Recent petrological compilations also indicate that subduction zones do not return blueschists and eclogites beyond 70–80 km on average (Agard et al., 2009; Guillot et al., 2009), possibly due to negative density

* Corresponding author.
E-mail address: samuel.angiboust@upmc.fr (S. Angiboust).

0024-4937/$ – see front matter © 2010 Elsevier B.V. All rights reserved.
doi:10.1016/j.lithos.2010.09.007

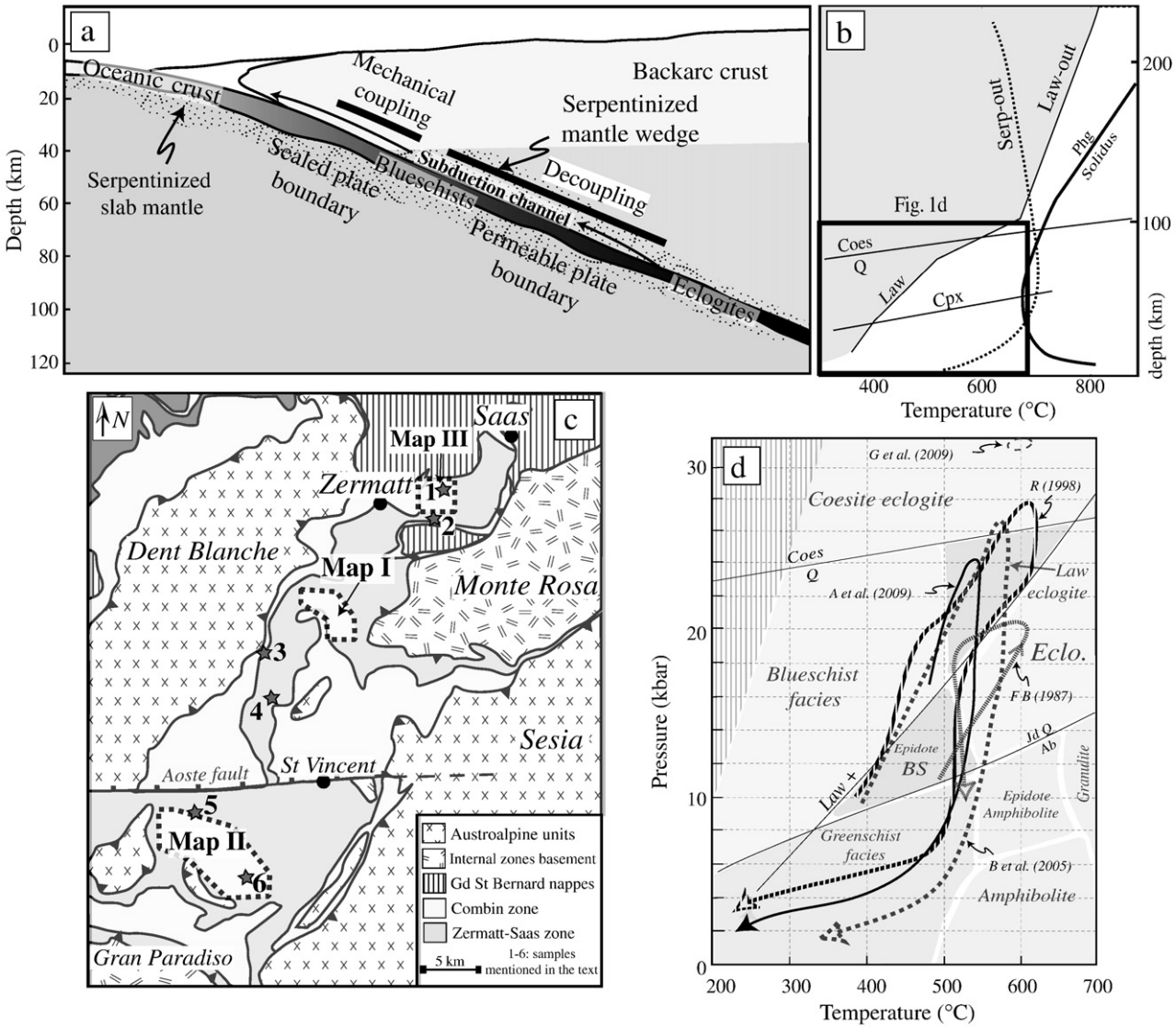

Fig. 1. a) Synthetic sketch featuring a subduction channel and the major characteristics of a subduction zone as inferred from recent geophysical data (modified after Onken et al., 2003; Audet et al., 2009). b) Key features of a petrogenetic grid showing the stability field of lawsonite and serpentinite for a MORB-type basalt (modified after Poli and Schmidt, 1995). c) Simplified geological map of the ZS ophiolite (modified after Baldelli et al., 1985), showing mapped areas and localizing the 6 main samples studied here. d) Compilation of the various published P–T paths from the literature for the ZS ophiolite (A: Angiboust et al., 2009; B: Bucher et al., 2005; FB: Fry and Barnicoat, 1987; G: Groppo et al., 2009; R: Reinecke, 1998). Background: main metamorphic facies. Mineral abbreviations: albite (Ab), coesite (Coes), lawsonite (Law), quartz (Q).

contrasts with the surrounding mantle, rheological weakening associated with fluid liberation or changes in the channel's structure.

Crustal (and mantle) slices hence likely migrate upwards along some sort of a channel, but the following questions remain: how do these rocks detach from the sinking slab, at which depth(s), what determines whether circulation occurs in a complex melange zone or as large-scale imbricated slices, to which extent are slab- or mantle wedge-derived serpentinites (or sediments) effectively present in the channel?

To address such questions we investigated the Zermatt–Saas ophiolite (ZS), one of the largest and deepest known, so far, portion of exhumed oceanic lithosphere (Bearth, 1966; Bucher et al., 2005; Angiboust et al., 2009). This highly hydrothermalized, mid-ocean type ophiolite, with abundant lawsonite pseudomorphs, also represents an ideal target to evaluate the influence of oceanic lithosphere on exhumation. In fact, although highly buoyant continental units underlying the ZS ophiolite (e.g. Monte Rosa unit), and mechanically weak serpentinites associated with mafic eclogites, are generally thought to account for the exhumation of this dense piece of oceanic lithosphere (Lapen et al., 2007; Agard et al., 2009), none of the other major ophiolite bodies from the same subduction zone (e.g., Pognante, 1985; Guillot et al., 2004; Voltri, Monviso, Rocciavre: Federico et al., 2007), shows the same characteristics (i.e., large-scale, continuous mafic slices and abundant lawsonite).

We herein report the results of new mapping, extensive sampling and rock/mineral chemistry on mafic protoliths from the whole ZS ophiolite, focusing on successive reequilibrations, lawsonite stability and fluid release through time. This approach is complemented by detailed thermodynamic modelling of the P–T evolution of these mafic protoliths. We show that hydrated phases significantly influence the buoyancy of the oceanic lithosphere and exhumation mechanisms and that the modelling of the ZS ophiolite P–T evolution provides critical constraints on the behaviour of mafic material and fluids deep in the subduction channel.

2. Geological background

2.1. Geological context and burial history

The ZS ophiolite, which extends from Saas-Fee area (Switzerland) to the Aosta valley (Italy; Fig. 1c), belongs to the internal Liguro–

Piemontese units of the Western Alps. It represents a fragment of the Mesozoic Neotethyan ocean subducted between c. 100 and 40 Ma below the Apulian margin (Dercourt et al., 1993; Rubatto et al., 1998; Amato et al., 1999; Dal Piaz et al., 2001; Agard et al., 2009).

These Liguro–Piemontese units comprise thrust sheets of non-eclogitic metasediments on top and on the western side (Combin zone), and predominantly mafic and ultramafic eclogitic bodies below and on the eastern side (Zermatt–Saas zone). Metamorphic grade thus broadly increases downwards (e.g., Bearth, 1967; Ballevre and Merle, 1993; Oberhansli, 2004).

Rocks from the Zermatt–Saas zone preserve a dismembered ophiolite sequence including manganiferous cherts, calcschists, pillow lavas, gabbros and serpentinites. Earlier petrographic, metamorphic and geochemical data were given by Bearth (1967, 1973), Chinner and Dixon (1973), Ernst and Dal Piaz (1978), Bearth and Stern (1979), Barnicoat and Fry (1986), Martin and Tartarotti (1989), Barnicoat and Cartwright (1995) and Van der Klauw et al. (1997).

P–T paths for the ZS zone indicate that the subducted oceanic crust underwent strikingly similar burial and exhumation patterns, at least 60 km across, and detached from the slab at depths around 70–80 km (~23–25 kbar, 530–550 °C; Fig. 1d; Angiboust et al., 2009). Serpentinized portions of the slab mantle underwent similar peak conditions (Li et al., 2004). Some small lenses may have reached greater depths however (~26–28 kbar), like the Lago di Cignana unit, where rare coesite inclusions within garnet and omphacite are known since the work of Reinecke (1991; see also recent estimates by Groppo et al., 2009).

These eclogitic fragments of this Liguro–Piemontese oceanic lithosphere (Monviso, Voltri, ZS) together with some rare continent-derived allochtons were subducted towards the end of the oceanic subduction, between c. 50 and 40 Ma (Duchene et al., 1997; Lapen et al., 2003, 2007; Beltrando et al., 2010). These eclogitic metaophiolites are closely associated with the underlying internal crystalline massifs (M. Rosa, G. Paradiso, D. Maira), where eclogite-facies lithologies are only found as relicts (e.g., Chopin and Monie, 1984; Le Bayon et al., 2006). Exhumation patterns are quite similar for both types of eclogites, oceanic and continental, as are relatively fast exhumation velocities (e.g., ~1–2 cm/yr; Amato et al., 1999; Lapen et al., 2007). Both rock types were significantly overprinted and deformed under blueschist facies conditions at 15–18 kbar during exhumation (Chopin et al., 1991; Michard et al., 1993; Schwartz et al., 2000; Guillot et al., 2004).

2.2. The ZS ophiolite: a large, hydrated fragment from a slow-spreading ocean

The mid-ocean ridge affinity of ZS eclogites was demonstrated geochemically by Bearth and Stern (1979), Dal Piaz et al. (1981), Pfeifer et al. (1989) and Barnicoat and Bowtell (1995). These metaophiolites have been discontinuously affected by hydrothermal oceanic alteration, with occurrences of Fe–Cu sulphide in metabasalts and Mn ore deposits in siliceous sediments (e.g., Dal Piaz et al., 1979; Tartarotti et al., 1986). Abnormal contents in various elements (Mg, Ca, and Na) and the scattering of $\delta^{18}O$ values are interpreted to reflect effects of hydrothermal processes and seafloor hydrothermal alteration of the oceanic crust (Cartwright and Barnicoat, 1999; Widmer et al., 2000; Martin et al., 2008).

Serpentinite breccias from the southern Aosta valley (Mont Avic area) described by Tartarotti et al. (1998) indeed suggest that oceanic mantle rocks were directly exposed on the ocean floor. This is in line with the conclusions from Lagabrielle and Cannat (1990) and Lemoine et al. (1987) that the Alpine oceanic crust was discontinuous, as for present-day slow-spreading ridges (Cannat et al., 1995). Tethyan slab mantle peridotites were in fact almost completely serpentinized as shown by the scarcity of the original mantle olivine remnants and the numerous rodingite dykes across the serpentinites (e.g., Ernst and Dal Piaz, 1978; Li et al., 2004).

Hydration of the oceanic lithosphere commonly occurs in the first two kilometers in the lavas, sheeted dikes, in the uppermost part of gabbroic layers (e.g., Dick et al., 2000) and even in the slab mantle (down to 10–20 km; e.g., Schmidt and Poli, 1998), particularly in slow-spreading ridges where the upper mantle is directly exposed on the seafloor (Seifert and Brunotte, 1996; Mével, 2003). This water, incorporated at mid-ocean ridges or along extrado faults during lithospheric bending before entering the trench (e.g. Ranero et al., 2003), mainly as serpentinite and chlorite (e.g., Cannat et al., 1992), is the main sink of water in the slab.

During subduction and recrystallization under eclogite-facies conditions, initial hydration and subsequent changes in bulk-rock composition allowed for the development of hydrous lithologies (chloritoschists, glaucophanites and talcschists) alternating with the anhydrous garnet–omphacite eclogitic assemblage (Oberhansli, 1982; Widmer et al., 2000). A compilation of bulk-rock composition analyses from different fresh, unretrogressed samples collected across the ZS ophiolite (Supplementary material A) shows that the water content in eclogites commonly ranges from 0.8–1.5 wt.% H_2O to 2–4% (glaucophanites), ~3% (talcschists) or 6–8% (chloritoschists). The complex history of seafloor weathering, also attested by strong modification of the ZS geochemical signature (Staudigel et al., 1996; Miller and Cartwright, 2000), thus led to the formation of an extensively hydrated reservoir able to release significant water amounts during subduction.

2.3. Ubiquitous lawsonite pseudomorphs

Lawsonite is one of the major carriers of water in subduction zones (Schmidt and Poli, 1998; Fig. 1b). Although experimental work and modelling suggest that lawsonite eclogite should be the dominant rock type for a typical oceanic subduction zone (e.g., Heinrich and Althaud, 1988; Poli and Schmidt, 1995; Clarke et al., 2006), they nevertheless only make a small fraction of eclogites exposed worldwide (see the recent review by Tsujimori et al., 2006). In many blueschist/eclogite belts, lawsonite was in fact retrogressed to epidote-bearing rhombic shaped aggregates during decompression and exhumation (e.g., Fry and Fyfe, 1971; Bearth, 1973; Ernst and Dal Piaz, 1978; Pognante, 1989; Ballevre et al., 2003).

Lawsonite was once very abundant and widespread in Zermatt–Saas metabasalts as shown by the preservation of mm- to cm-sized pseudomorphs in the whole ophiolite unit (Täsch valley: Bearth, 1966; Fry and Fyfe, 1971; Fry and Barnicoat, 1987; Valtournanche: Ernst and Dal Piaz, 1978; Saint-Marcel valley: Martin and Tartarotti, 1989). Complexity in textural relationships between the matrix and these pseudomorphs, however, led to ambiguities on inferred P–T trajectories and on the stability history of lawsonite. Martin and Tartarotti (1989) advocated for two stages of lawsonite stability, separated by lawsonite-free eclogitic conditions. In contrast, several authors, based on the lack of pseudomorphs included in garnet and on the existence of only weakly deformed matrix pseudomorphs (Bearth, 1973; Barnicoat and Fry, 1986; Barnicoat, 1988), assumed that lawsonite crystallized in metabasalts after eclogitic peak conditions. According to them, post-eclogitic lawsonite growth resulted from isobaric cooling during the first part of the return path, before isothermal decompression and subsequent lawsonite breakdown (Fig. 1d).

3. Structural and petrological observations

3.1. Tectonic slices and structural patterns

The ZS unit is mainly composed of serpentinites (about ~45% of the outcrops surface), mafic rocks (metabasalts and hydrothermalized metabasalts, metagabbros and ophicalcitic breccias; ~40% of the

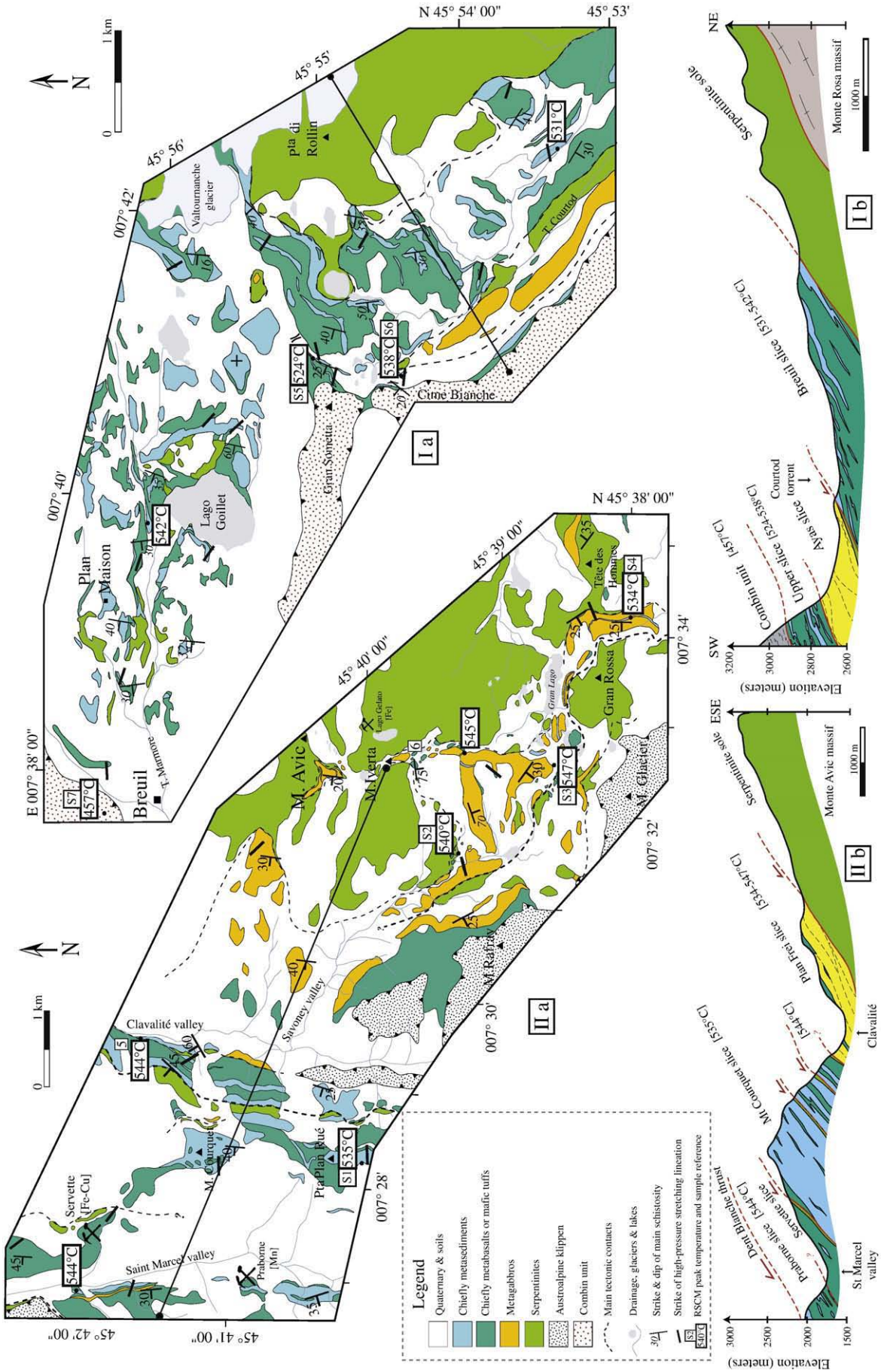

Fig. 2. Geological maps and cross-sections of the three main areas investigated here (see Fig. 1c for location: Mont Avic, Breuil-Ayas and Täsch areas). All three areas show the stacking of eclogite-facies nappes over a thick serpentinite sole.Map I is based on our field observations. Field observations for map II have been complemented, for Monte Raffray area, by the Geological Map of Chatillon (Dal Piaz et al., in press; 1/50,000 scale). Map III is based on our field observations, combined with ealier mapping from Bearth (1964) and Fry and Barnicoat (1987). Note that most slices are separated by a 5 to 50 m thick serpentinite sliver. High-pressure stretching lineations (arrows) and RSCM peak temperature estimates (Table 2 and Section 3.4 for details) are also shown.

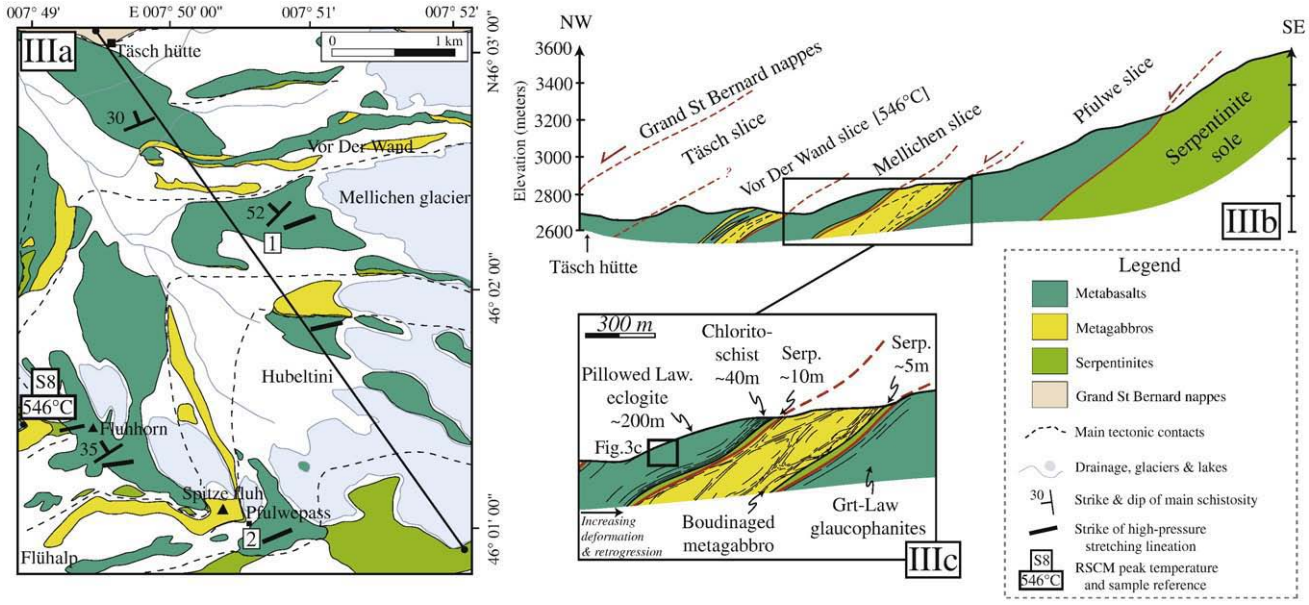

Fig. 2 (*continued*).

ophiolite) and minor sedimentary lenses (calcschists, mafic schists and metacherts; <15%).

The internal tectonic structure of the ZS ophiolite is poorly constrained. New mapping and extensive fieldwork investigations across the ZS ophiolite led to the recognition of several tectonic slices, which are systematically separated by a variably thick layer of strongly deformed serpentinite (from a few meters to 100–200 m; Fig. 2; Table 1). These slivers of mylonitized serpentinite within shear zones commonly exhibit talc-, chlorite- and tremolite-bearing schists (Martin et al., 2008). Shearing during HP metamorphism is marked on the field by early top-to-the-west shear zones which could correspond to deep thrusts in the subduction zone, as argued by Fry and Barnicoat (1987; Fig. 2). Early shear criteria along these thrust planes are obscured, however, by exhumation-related extensional movements (Ballevre and Merle, 1993; Wheeler and Buttler, 1993; Barnicoat et al., 1995; Cartwright and Barnicoat, 2002).

The rocks making up theses slices have a highly variable content in metasediments from close to 0% in Mellichen or Pfulwe slices (Täsch area, Fig. 2 III) to ~60% in Mont Courquet slice (St-Marcel–Clavalité areas, Fig. 2 II; Table 1). In all studied slices, we found evidence for undisturbed stratigraphic contacts between the metabasalts and the sediments. Manganiferous quartzites, in particular, mark the location of palaeo-oceanic floor and are commonly associated with pillow relicts, breccias and hyaloclastites (see Dal Piaz et al., 1979; Bearth and Schwander, 1981 for further details). Some mafic layers embedded within the sedimentary groundmass are also commonly flattened, stretched and boudinaged.

Metagabbroic bodies are strongly retrogressed, boudinaged and mylonitized on their margins, particularly in the lower part of the slice. The gabbro slice lying along the Savoney valley (Fig. 2 IIa) is composed of 100–200 m thick boudinaged lenses separated by 2–40 m thick serpentinite layers (locally interleaved with calcschists) concentrated on the edges of the gabbro slice. In Täsch area (Fig. 2 IIIc), the gabbro slice is strongly boudinaged and separated from the adjacent metabasaltic units by thin mylonitized serpentinite slivers. The bottom part of the Mellichen slice is also strongly retrogressed to chloritoschists suggesting widespread fluid circulation at the contact with the gabbro.

The 150–500 m thick ophiolite slices (e.g., Fig. 2 IIb, IIIb) are systematically underlain by a thick (>500 m) serpentinite sole (Fig. 2). Some serpentinite soles are devoid of crustal slices, as in Täsch (Fig. 2 III) and Breuil–Ayas areas (Fig. 2I). Near Mont Avic (Fig. 2 II), only rare dismembered gabbroic bodies are disseminated in the upper part of the serpentinite sole (e.g., gabbro of "Tête des Hommes", Fig. 2 IIa). We note, however, that the distribution of serpentinite sedimentary breccias (Tartarotti et al., 1998) may suggest the existence of several intra-sole thrust slices within the 15-km large ultramafic dome of the Mt Avic massif. The contact between the serpentinite sole and the crustal stack above is also locally folded, yet possibly as a result of later collisional folds.

In all studied areas uppermost slices close to upper shear zones (e.g., Combin shear zone, Dent Blanche, and Grand St Bernard) are more pervasively affected by a greenschist facies overprint than the slices located deeper in the ophiolite stack (e.g., Praborna slice in St-

Table 1
Field-based estimates of crustal lithology proportions and overall density for each ZS tectonic slice. Calcschist density under peak conditions (3071 kg m^{-3}) was calculated using pseudosection modelling on a representative calcschist sample composition. See text for details (and Section 6.3 for a discussion of their respective buoyancy).

Area/slice name	Field estimation of the slice composition (vol.%)		Slice thickness (meters)	Typical assemblage in fresh eclogitized metabasalts	Ave. Law abundance (vol.%)	Ave. H_2O (vol.%) in eclogites	Ave. eclogite density	Ave. slice density
	Calcschists	Metabasalts						
Breuil	35	65	400–500	Grt–Gln–Law ± Omp ± Phg ± Dol ± Ep	3%	1.5–2.0	3400	3285
Mellichen	5	95	200–300	Grt–Gln–Law ± Omp ± Dol ± Ep ± Phg	10%	1.5–2.5	3350	3336
Pfulwe	2	98	250–350	Grt–Omp–Gln ± Law ± Ctd ± Tlc	12%	1.5–3.5	3350	3344
Praborne	20	80	350–450	Grt–Gln–Law ± Omp ± Ep	4%	1.5–2.0	3300	3254
Courquet	60	40	600–800	Grt–Gln–Law ± Omp ± Ep	6%	1.5–2.0	3350	3183
Clavalité	35	65	250–300	Grt–Gln ± Law ± Ctd ± Tlc ± Omp	5%	2.0–3.0	3300	3220
Servette	10	90	200–250	Grt–Gln–Law ± Ctd ± Tlc	8%	2.0–3.0	3350	3322

Marcel area, Fig. 2 IIb; Upper slice in Breuil–Ayas area, Fig. 2 Ib; Täsch slice in Täsch area, Fig. 2 IIIb; Fig. 3a).

Different lineation sets were measured on the field. Earliest lineations, marked by elongated omphacite or lawsonite are generally weak and blurred by a later epidote blueschist or greenschist facies overprint. Most HP lineations range between N100 and N140 in Breuil–Ayas area (Fig. 2 Ia), and between N90 and N130 in the St-Marcel–Clavalité area (Fig. 2 IIa). Structural patterns are more complex in the Mont Avic–Raffray area (Fig. 2 IIa), where stretching lineations span a broad range in the dismembered portions of the metagabbroic body. HP lineations cluster in Täsch area between N75 and N90 (Fig. 2 IIIa). Even if these stretching lineations point to E- or SE-directed thrusting some of them may have been re-oriented by later deformation events (e.g., Wheeler et al., 2001).

3.2. Textural observations of metabasalts

Metabasalts of the ZS ophiolite identified as zoned N-MOR basaltic pillow lavas (Bearth, 1959; Dal Piaz et al., 1981) display considerable textural and mineralogical variations, which may be due to contrasting post-eclogitic events and/or ocean-floor processes (Oberhansli, 1982; Barnicoat and Bowtell, 1995). Ocean-floor hydrothermal alteration produced widespread chemical zonation of pillows-lavas which led to the development of glaucophane-rich rims around eclogitic cores (named "classical metabasalts" in this study). Such apparent changes in metamorphic grade between eclogites and blueschists over distances of a few centimeters thus unlikely reflect variations in HP metamorphism but rather relate to variations in bulk-rock chemistry.

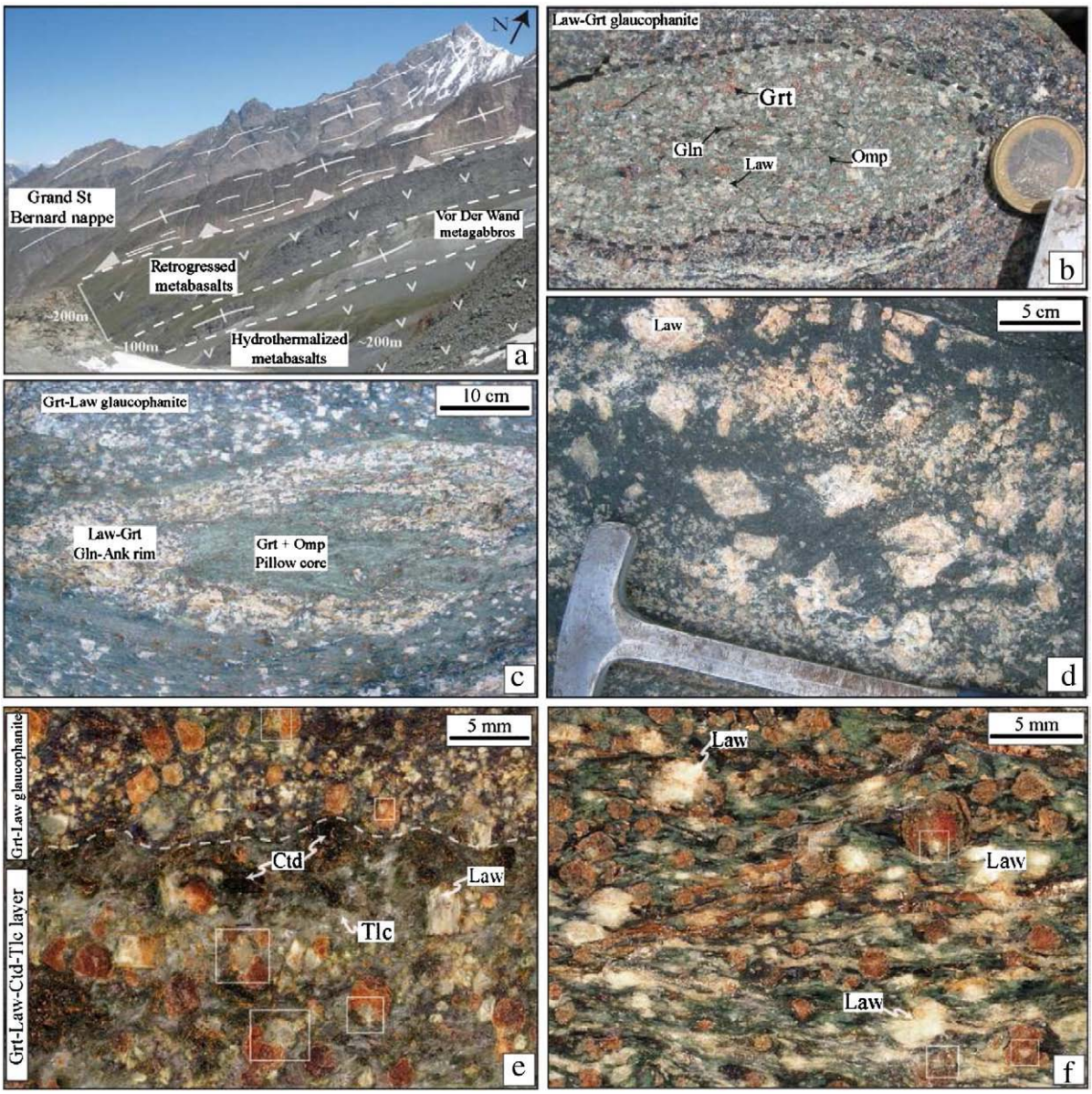

Fig. 3. a) Field view over the Täschalp area (map 1, Figs. 1 and 2), where a stack of 100–200 m thick slices of oceanic crust crop out below the Gd St Bernard nappe. b) Boudinaged Grt–Omp–Law–Gln layer in Law–Grt glaucophanites from locality 6 (Fig. 1). Note that mineral abbreviations, hereafter, are after Kretz (1983), except for chloritoid (Ctd), lawsonite (Law), quartz (Q) and phengite (Phg). c) Relict of a zoned, eclogitized pillow basalt with dry assemblages (Grt + Omp) concentrated in the core, whereas hydrated assemblages (mostly pseudomorphs after lawsonite and glaucophane) are concentrated on the rims (locality 2, Täsch valley). d) Glaucophanite with up to 5 cm-long lawsonite pseudomorphs, 500 m west of Pfulwepass (locality 2). e) Typical Mg-rich hydrothermalized metabasalt with Grt–Law–Ctd–Tlc vein cross-cutting a matrix of Grt–Law glaucophanites. Note that lawsonite is abundant both in the matrix or included within garnet rims (white squares) in both lithologies (locality 5). f) Law eclogite from the southern edge of Lago Di Cignana (locality 3). Note that pseudomorphs after lawsonite are commonly included within garnet rims (white squares). Other phases include omphacite, which defines the main peak foliation, and glaucophane which occurs as rims around garnet or in the foliation between omphacite.

On the other hand, most of the ZS ophiolite rocks do not follow identifiable original structures such as pillows but more commonly display as irregularly shaped 10 cm to a few meters long eclogite patches rimmed by glaucophanites (Fig. 3b). In such lithologies, the respective contributions from original bulk-chemistry variations and from boudinage of eclogitic relicts under blueschist facies conditions cannot be assessed.

We present later the results of observations made on more than 100 thin-section specimens, mostly on classical metabasalts (but also on highly hydrothermalized magnesian metabasalts; see discussion later). Abbreviations used in this work are after Kretz (1983) except for lawsonite (Law), quartz (Q), chloritoid (Ctd) and phengite (Phg).

3.2.1. Classical metabasites

Classical metabasalts of the ZS unit are particularly suited for our study because the high-grade upper part of their P–T path is well-preserved. Early metamorphic evolution within classical metabasites is attested by the upper-blueschist assemblage of Gln ± Law ± Ep ± Dol − Rt inclusions in the cores of garnet porphyroblasts. Mm- to cm-large garnet porphyroblasts are texturally, mineralogically and chemically zoned with Mn- and Ca-enriched cores and Fe- and Mg-enriched rims. Disappearance of amphibole and appearance of omphacite needles and quartz grains within garnet rims characterizes the blueschist to eclogite transition accompanying the burial of the ophiolite.

Eclogitic matrix is characterized by elongated omphacite crystals aligned along the main foliation, wrapping garnet and lawsonite porphyroblasts (Fig. 3e,f). Omphacite occurs in some eclogites as tails on garnet or lawsonite. In some samples (Fig. 4a), a second omphacite-bearing foliation (Omp II) overprints a previous eclogitic foliation, wrapping the garnetI–omphaciteI–lawsonite porphyroblast. Phengite is randomly disseminated within garnet and is aligned in the matrix along the dominant omphacite fabric. Quartz is found dominantly in garnet pressure fringes. In some samples, glaucophane and epidote are stable with eclogitic assemblages as suggested by their alignment within the eclogitic matrix. In glaucophane-rich samples, contrary to classical Grt-Omp-Law eclogites, glaucophane is commonly included within garnet rims. Kyanite has never been observed in classical metabasites. Rutile and sulphides may be abundant (up to 1–2 vol.%) in some samples. Oxides have not been observed within fresh eclogite-facies samples.

Early exhumation of these rocks is marked by fine Ca-rich overgrowths on omphacite, and is likely coeval with the locally strong epidote-blueschist facies foliation wrapping around eclogitic boudins, (~500 °C, 15–18 kbar; Angiboust et al., 2009). Glaucophane crystallizes as very thin needles at the boundary between garnet and omphacite. Unlike glaucophane inclusions in omphacite and garnet rims, these glaucophane crystals are clearly the product of re-equilibration of eclogites during exhumation. In places, this blue-amphibole foliation is accompanied by mm-sized aggregates of epidote and interstitial paragonite. Lawsonite breakdown and lawsonite pseudomorph textures will be discussed in the next section.

Under greenschist facies conditions omphacite is affected by widespread and thorough symplectitic recrystalizations (generally albite and magnesio hornblende), garnet is retrogressed by chlorite (and rarely by biotite), while blue-amphibole is destabilized by greenish Ca–Na amphiboles. Titanite commonly replaces rutile in the most retrogressed lithologies.

3.2.2. Magnesian metabasites

Magnesian metabasites found in the southern Aosta valley and in the Pfulwepass area (Fig. 2 II,III) show unusual high-pressure lithologies: garnet glaucophanites, talcschists and chloritoschists (Martin and Tartarotti, 1989; Widmer et al., 2000; Bucher et al., 2005; Fig. 3e). In the chloritoid-talc rich layers interbedded with garnet glaucophanites of St-Marcel and Clavalité areas (Fig. 2 II), cm-sized garnet porphyroblasts host numerous inclusions in support of the prograde paragenesis garnet + chloritoid + quartz + glaucophane ± epidote ± chlorite ± talc ± lawsonite. The typical HP matrix assemblage within these thin layers is characterized by garnet, chloritoid, talc ± omphacite and locally lawsonite and glaucophane.

These highly hydrated magnesium-rocks, although interesting in terms of petrology and hydrothermal processes, are nevertheless volumetrically insignificant with respect to the rest of the ophiolite. We therefore focused our attention on the predominant classical metabasalts, which are representative of the average mafic material in the subduction channel. P–T pseudosections for the more magnesian lithologies can be found in the literature (Bucher et al., 2005; Martin et al., 2008; Wei and Song, 2008).

3.3. Lawsonite pseudomorphs

At the outcrop scale, lawsonite pseudomorphs are irregularly distributed within fresh eclogites and garnet glaucophanites (Fig. 3b, c). Although modal proportions range from 0 to 20 vol.% in the eclogites, most metabasalts contain between 5 and 10 vol.% lawsonite pseudomorphs. Lawsonite, associated with carbonates, is also abundant (up to 30 vol.%) in cm-sized garnet–omphacite-bearing veins cutting across eclogites boudins in Täschalp area. Interestingly, in the same area, some fractures are lined up with elongated and rosette-shaped pseudomorphs after lawsonite (as already described by Fry and Barnicoat, 1987). On the Fluehorn ridge, west of Pfulwepass, the thrust contact between a metabasalt slice and a gabbro slice exposes particularly large and abundant lawsonite pseudomorphs (up to 6 cm-long, Fig. 3d). The size and abundance of these pseudomorphs decrease away from the contact towards the middle of the metabasalt slice to reach the typical lawsonite abundance in ZS slices (i.e., ~10 vol.% and 0.5–1 cm in length). Such large pseudomorphs have also been observed within metabasalts 10 m beneath the boundary between the Vor der Wand gabbro slice and the Mellichen eclogitized pillows slice (Figs. 2 III, 3a). The lawsonite content of eclogites also seems to increase towards basalt–sediment boundaries in eclogites and glaucophanites from Breuil and St-Marcel areas.

Under the microscope, lawsonite pseudomorphs occur both in the matrix and in garnet rims, but are more rarely preserved within omphacite (Figs. 3f, 4a,b,g; Angiboust et al., 2009). Although breakdown products proportions vary between samples, epidote makes up 80 vol.% of the pseudomorphs on average, while paragonite abundance is 5 to 15 vol.% (Fig. 4). Small amounts (<5 vol.%) of accessory chlorite, quartz and albite occasionally coexist with epidote and paragonite (Fig. 4g).

In classical eclogite-facies metabasalts, pseudomorphs are euhedral and aligned along the main omphacite fabric (Fig. 3b,f). In the less deformed and retrogressed samples, some of the pseudomorphs preserved their distinctive rectangular shape (Fig. 4f). Locally, a secondary omphacite foliation is deflected around lawsonite porphyroblasts (Fig. 4a,f). In this sample (ZS0716-locality 4), pressure shadows around lawsonite porphyroblasts, hosting quartz or phengite, are locally filled by a secondary fine-grained omphacite. In structures interpreted as pillow lava relicts (Fig. 3c), lawsonite pseudomorphs are mainly associated with garnet and omphacite in the outer pillow cores, while lawsonite grows with glaucophane, epidote and dolomite in the rims (Fig. 3c). Within samples strongly overprinted by blueschist or greenschist facies, the glaucophane foliation is often deflected around the porphyroblastic pseudomorphs (Fig. 4e).

In magnesium-rich metabasalts, lawsonite pseudomorphs expose typical lozenge-shaped habitus and are included within garnet cores and rims (Figs. 3e, 4d,e). Lawsonite has never been included within chloritoid.

Several interesting textural patterns were observed in lawsonite pseudomorphs. Some host inclusions, such as omphacite in the cores

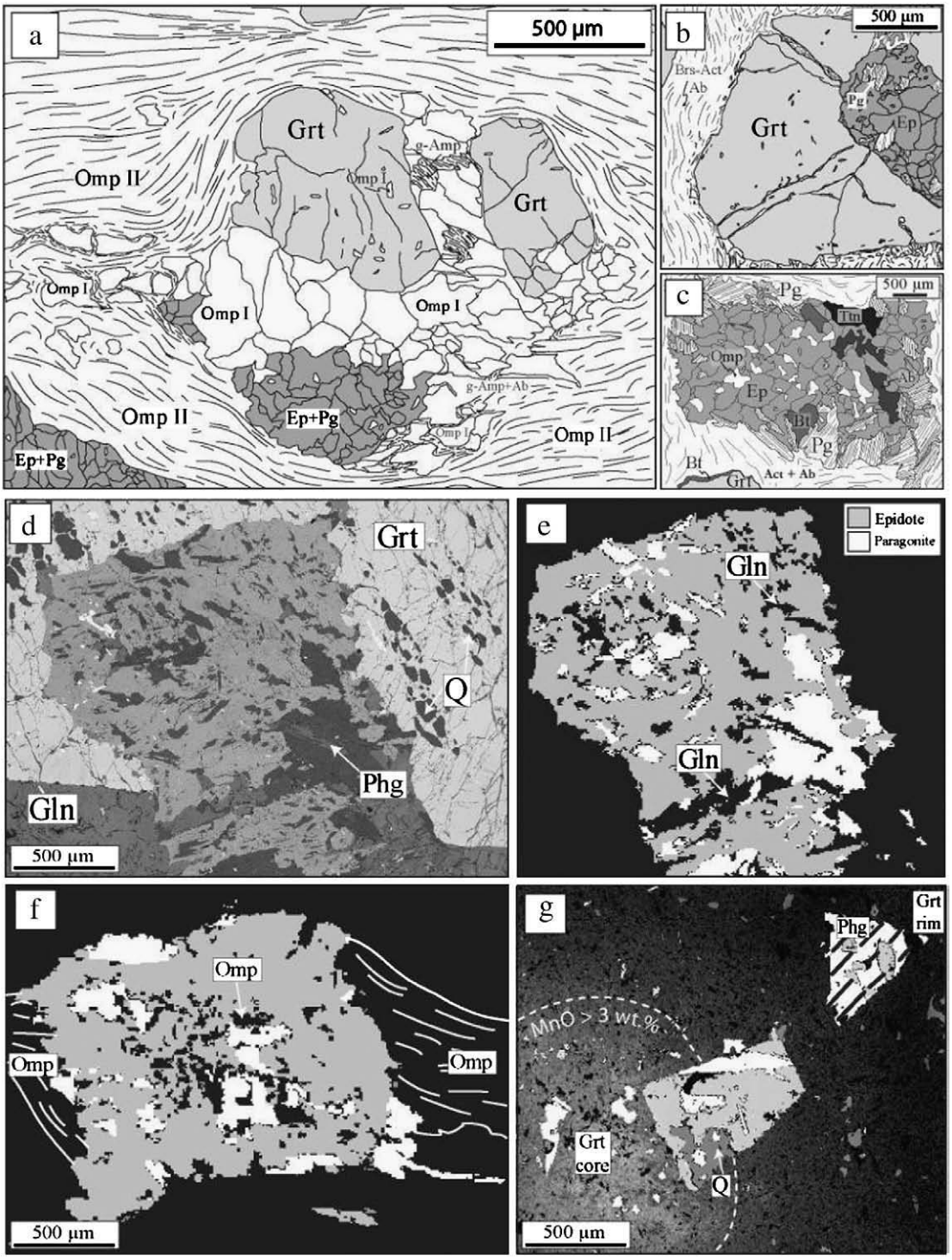

Fig. 4. a–c) Optical microscope sketches underlining the textural relationships between lawsonite pseudomorphs and the surrounding matrix: a) relict of a peak Grt–Omp–Ep–Pg aggregate (the latter two represent a pseudomorph after Law) wrapped by a secondary omphacite-bearing foliation (eclogite, locality 4). b) Quadrangular aggregate of epidote and paragonite included within a garnet core (eclogite, locality 4). c) Quadrangular aggregate of Ep + Pg (the latter being concentrated on the rim of the pseudomorph). Omphacite inclusions (Omp) are rather concentrated in the core of the pseudomorph. Late reequilibration triggered the formation of albite, actinolite and biotite in the pseudomorph, in the matrix and on the garnet rims (eclogite, locality 2). d) SEM picture showing a quadrangular aggregate of Ep + Pg + Phg with glaucophane inclusions in a garnet rim from sample 5 (Clavalité valley). e–g) Lawsonite pseudomorph mineralogy revealed by image processing of SEM pictures (epidote and paragonite masks are grey and white, respectively): e) relative proportions of epidote and paragonite from the SEM image of picture (d). f) Lawsonite pseudomorph wrapped in an omphacite-bearing foliation underlined by thin white lines (locality 4, Valtournanche): note that older omphacite crystals are concentrated in the core of the pseudomorph. g) Lawsonite pseudomorph from Lago di Cignana (locality 3) included in the Mn-rich domain of a garnet.

(Fig. 4f) of glaucophane needles on the outer edge of the pseudomorphs (Fig. 4e). Mineralogical zonation may also occur with epidote-rich cores surrounded by paragonite-rich rims (Fig. 4c) next to the omphacite matrix.

3.4. The metamorphic record of metasediments

The ZS ophiolite exposes a broad variety of metasediments with impure marbles, cherts, calcschists, quartzites, mafic tuffs and mafic

Table 2
Summary of maximum temperatures inferred from the Raman spectroscopy of carbonaceous material from various calcschists (RSCM, Beyssac et al., 2002; sample location in Fig. 2). R^2 ratio with temperatures (T) in °C and 1σ standard deviation (SD). n: Number of spectra acquired for each sample from ZS ophiolite (ZS) or from the adjacent Combin unit (CO).

Samp.	n	R^2	T	SD
S1 (ZS)	12	0.24	535	14
S2 (ZS)	12	0.23	540	18
S3 (ZS)	13	0.21	547	26
S4 (ZS)	12	0.24	535	16
S5 (ZS)	12	0.26	524	12
S6 (ZS)	13	0.23	538	17
S7 (CO)	16	0.41	457	18
S8 (ZS)	13	0.21	546	28

schists. The lowest variance peak assemblages recorded are some calcschists containing garnet, phengite and chloritoid (±lawsonite pseudomorphs). Raman spectroscopy of carbonaceous material (geothermometer of Beyssac et al., 2002) of these calcschists gave peak temperatures estimates comprised between 523 and 545 °C in a previous study (Angiboust et al., 2009). Following the same method, we performed 8 new analyses on calcschists from different slices in order to evaluate the homogeneity of maximum temperature within the slice stack (Table 2; location on Fig. 2).

4. Rock and mineral chemistry

Details regarding analytical techniques and procedures (whole-rock chemistry, microprobe and Raman spectroscopy) are given in Appendix A.

4.1. Bulk-rock composition of ZS samples

Seafloor weathering and active hydrothermal circulation can modify pervasively the bulk-rock chemistry of newly formed oceanic crust (Seyfried et al., 1978; Mottl, 1983). Seafloor alteration strongly depends on alteration temperature, fluid chemistry and water/rock ratios (see also experimental data of Mottl, 1983; Seyfried et al., 1978 for a complete discussion) and generally implies a relative enrichment in MgO, K_2O and Na_2O in the pillow rim whereas CaO is leached out by seawater (e.g., Seifert and Brunotte, 1996).

In contrast to the very low H_2O content of fresh oceanic basalts (<0.5 wt.%; e.g., Jambon and Zimmermann, 1990), 2–3 wt.% of water are commonly added to oceanic crust undergoing hydrothermal seawater alteration (Harper et al., 1988; Staudigel et al., 1996), and up to 10–15 wt.% H_2O can be incorporated by the crystallization along pillow rims and fractures, of strongly hydrated secondary minerals such as zeolites, chlorite, talc or smectites.

In order to evaluate the representativity of our rock compositions, bulk-rock chemical analyses are projected in an AFM diagram (Fig. 5). Our analyses plot in the same field as those of Widmer et al. (2000) for "classical" eclogites and for "magnesian" metabasalts see also Martin et al., 2008 and references therein).

All the ZS classical eclogites show a noticeable enrichment in Na (and to a lesser extent K) with respect to MORB composition probably as the result of low temperature fluid-rock interactions (mostly spilitization). A strong higher temperature hydrothermal alteration (chloritization) locally gave rise to the very peculiar parageneses observed in eclogitized Mg-metabasalts from St-Marcel, Clavalité, Pfulwe areas and described earlier (Barnicoat and Bowtell, 1995; Widmer et al., 2000; Bucher et al., 2005; Martin et al., 2008).

4.2. Mineral analyses

The average garnet composition within classical metabasites is $Alm_{55-65}Grs_{25-35}Py_{5-12}Sps_{2-4}$ (n = 270) while it is $Alm_{50-55}Grs_{15-20}Py_{20-25}Sps_{1-3}$ (n = 495) within Mg-rich metabasalts (Pfulwe and Allalin gabbros analyses) and $Alm_{70-80}Grs_{6-15}Py_{6-13}Sps_{1-6}$ within Fe–Mg-rich metabasalts from southern Aosta valley area (see Table 4 for representative mineral compositions). Core-rim zonation, which are particularly sharp within Mg-metabasalts from the southern Aosta valley (e.g., Angiboust et al., 2009), shows typically Ca- and Mn-enriched cores and Fe- and Mg-enriched rims (Fig. 4g).

Omphacite contains between 45 and 60% jadeite component and has an average X_{Mg} of 0.72 (σ = 0.1, n = 130 analyses). The average composition of omphacite is $Di_{47}Jd_{47}Ac_6$. Acmite component is relatively low across the ophiolite (1–12%), except for some glaucophanite–eclogites slices in the Mont Avic massif (southern Aosta valley) where an average omphacite composition ($Jd_{50}Di_{35}Ac_{15}$) suggests higher Fe^{3+} activities (Table 4). Omphacite is rarely zoned, except in Lago di Cignana eclogites where omphacite cores are slightly richer in jadeite (~52%) than the rims (~47%). Omphacite cores and omphacite as inclusions within garnet rims are slightly richer in jadeite component than the rim. Omphacite needles included within pseudomorphs after lawsonite are chemically similar to omphacite from the matrix (Fig. 4f).

Microprobe analyses of amphibole were recalculated according to the procedure outlined by J. Schumacher (in Leake et al., 1997). High-pressure amphibole is systematically sodic and close to end-member glaucophane composition with average X_{Na} of 0.95 (σ = 0.05, n = 85) and X_{Mg} ranging from 0.6 to 0.8. Peak amphibole and post-eclogitic amphibole are chemically similar. Fe^{3+} content of glaucophane is particularly low in ZS metabasalts (X^{3+}_{Fe} ~4%, σ = 6%; Table 4). Ca–Na amphibole occurs either as thin rim around glaucophane or as very fine-grained intergrowths with albite in symplectites around omphacite. In classical metabasalts, Ca–Na amphibole corresponds to barroisite whereas winchite is prevalent in hydrothermalized magnesian metabasalts. In the most retrogressed samples, needles of Ca-amphibole (mainly actinolite and magnesiohornblende) form in the matrix and as fine overgrowths around pyroxene and barroisite.

Epidote analyses from metabasites from the ZS ophiolite do not show significant zonation, and have a pistacite component between 8 and 22%. Early, peak and retrograde epidote after lawsonite show similar compositional patterns.

Phengite is mostly present in slightly altered classical metabasalts or within interpillow material. In fresh eclogites, phengite has Si

Table 3
ICP-AES and ICP-MS major element bulk-rock analyses for metabasalts sampled across ZS ophiolite (see Fig. 1 for sample location).

Sample	SiO_2	Al_2O_3	FeO	MnO	MgO	CaO	Na_2O	K_2O	TiO_2	P_2O_5	LOI	Total	Loc.	Rock type
ZS0833	46.78	16.58	9.68	0.16	7.29	9.75	3.32	0.34	1.98	0.14	1.0	98.37	3	Law–Gln eclogite
ZS0865b	49.87	16.85	12.37	0.25	5.42	6.16	4.66	0.13	2.37	0.34	0.8	99.21	6	
ZS0708	52.01	17.68	8.00	0.13	4.17	11.82	3.02	0.29	1.68	0.20	0.8	99.80	3	
ZS0909	50.00	16.91	8.37	0.16	7.80	8.60	4.48	0.04	1.40	0.14	1.6	99.50	1	
ZS0926	46.60	16.72	11.67	0.26	5.50	9.87	3.78	0.76	2.25	0.04	0.6	98.05		Law–Phg ecl.
ZS0716b	49.49	16.89	6.53	0.12	6.26	12.16	4.44	0.06	1.26	0.17	1.0	98.37	4	Law eclogite
ZS0715b	47.56	17.72	6.33	0.13	6.17	10.25	4.89	0.11	1.48	0.21	1.5	96.35	4	
ZS0904	45.46	18.21	11.47	0.37	11.76	5.41	2.82	0.00	1.15	0.29	2.5	99.44	2	Mg metab.
ZS0721b	55.25	15.00	7.34	0.19	10.75	4.83	3.26	0.10	1.77	0.27	2.4	101.15	5	

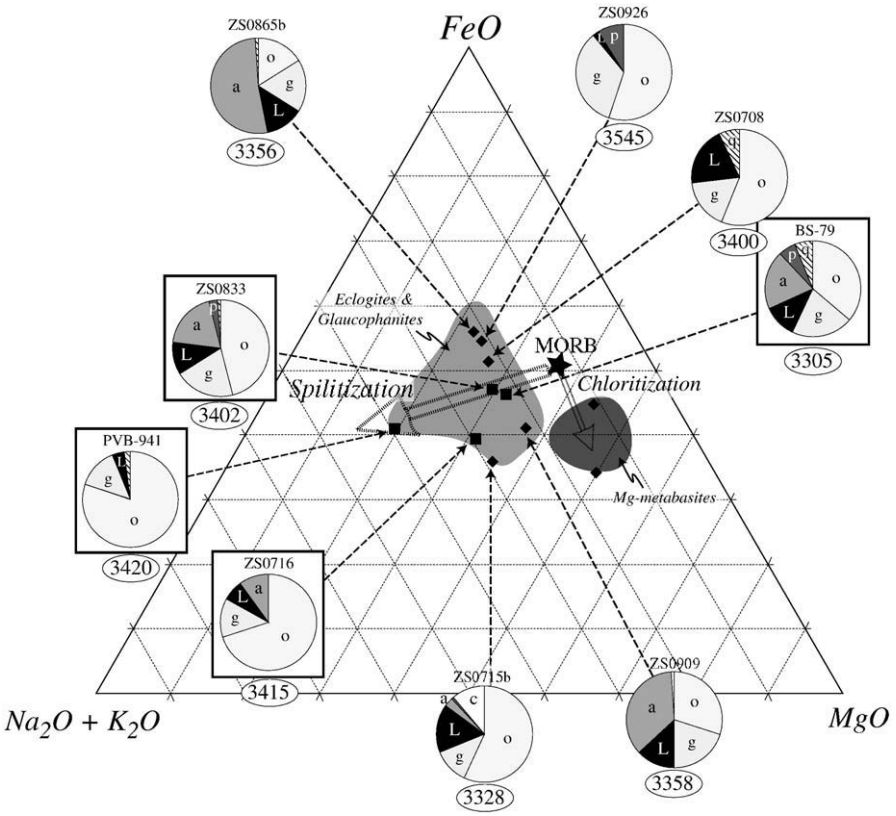

Fig. 5. Plot of bulk-rock compositions in a modified AFM diagram (alkalis versus MgO and FeO). MORB composition after Hacker et al. (2003a). Grey overlays: typical spread of MORB compositions resulting from spilitization and chloritization, respectively (eclogites and glaucophanites in light grey, and Mg-rich metabasites in dark grey, respectively; after Widmer et al., 2000). Circle charts represent calculated peak proportions in vol.%. Those outlined by squares correspond to the rocks for which pseudosections were calculated (Fig. 6). Calculated densities of the corresponding, eclogitized metabasalts are also shown (at 550 °C–24.5 kbar under water-saturated peak conditions). Mineral abbreviations: a: glaucophane, c: chlorite; g: garnet; o: omphacite, L: lawsonite, p: phengite, q: quartz.

Table 4
Table of selected microprobe analyses of omphacite, garnet, phengite and glaucophane from ZS eclogite samples.

Locality	3	6	4	3	6	4	3	4	3	4
Sample	ZS0833	ZS0865b	ZS0716	ZS0833	ZS0865b	ZS0716	ZS0833	ZS0716	ZS0833	ZS0716
Mineral	Omp			Grt			Phg		Gln	
Num.	h191	o6	n108	h189-11	o11	n95	h209	o85	h210	o142
Location	S	S	inc grt	mid	rim	rim	S	ps. Law	S	S
SiO_2	57.03	55.91	56.09	38.50	37.17	37.54	53.88	51.70	57.38	59.18
TiO_2	0.04	0.08	0.12	0.22	0.09	0.11	0.29	0.20	0.04	0.00
Al_2O_3	10.73	10.10	10.14	21.11	20.24	22.40	24.02	25.22	11.72	11.71
FeO_T	5.16	10.22	6.32	27.38	32.74	27.57	2.02	1.53	8.43	7.02
MnO	0.03	0.00	0.00	0.86	0.73	0.71	0.02	0.02	0.00	0.02
MgO	7.91	5.27	7.29	3.35	2.36	3.98	4.85	3.79	11.49	11.99
CaO	12.00	8.52	12.73	8.99	6.63	7.87	0.00	0.02	2.05	0.72
Na_2O	7.88	8.94	6.78	0.00	0.05	0.00	0.23	0.36	6.42	7.07
K_2O	0.00	0.00	0.00	0.03	0.00	0.00	10.00	10.43	0.01	0.00
Sum	100.77	99.05	99.46	100.43	100.01	100.18	95.32	93.27	97.54	97.69
Si	2.02	2.05	2.02	3.02	3.00	2.95	3.57	3.50	7.85	7.99
Ti	0.00	0.00	0.00	0.01	0.01	0.01	0.01	0.01	0.00	0.00
Al	0.45	0.44	0.43	1.95	1.92	2.07	1.87	2.02	1.89	1.86
Fe^{2+}	0.06	0.16	0.19	1.80	2.11	1.81	0.11	0.09	0.78	0.61
Fe^{3+}	0.09	0.15	0.00	0.01	0.09	0.00	0.00	0.00	0.17	0.17
Mn	0.00	0.00	0.00	0.06	0.05	0.05	0.00	0.00	0.00	0.00
Mg	0.42	0.29	0.39	0.39	0.28	0.47	0.48	0.38	2.34	2.41
Ca	0.45	0.33	0.49	0.76	0.57	0.66	0.00	0.00	0.30	0.10
Na	0.54	0.63	0.39	0.00	0.01	0.00	0.03	0.05	1.70	1.85
K	0.00	0.00	0.00	0.00	0.00	0.00	0.84	0.90	0.00	0.00
X_{Jd}	0.45	0.46	0.47							
X_{Acm}	0.09	0.16	0.00							
X_{Prp}				0.13	0.09	0.16				
X_{Alm}				0.60	0.70	0.60				
X_{Mg}	0.73	0.48	0.67	0.18	0.12	0.21	0.81	0.81	0.75	0.80

contents mostly in the range 3.45–3.58 per formula unit. Paragonite is more abundant within both types of metabasalts, and mostly occurs as pseudomorphs after lawsonite. Paragonite shows a restricted range of composition from $Pg_{90}Mu_8Cel_2$ to $Pg_{96}Mu_3Cel_1$ whatever its textural position.

Chlorite analyses span a range from $Clin_{82}Ames_{12}Sud_6$ to $Clin_{65}Ames_{30}Sud_6$. Chlorite, which is widespread within Mg-metabasalts, shows lower X_{Mg} values when included within garnet cores than when growing at the expanse of garnet or chloritoid during late retrogression.

5. Modelling the mineralogical evolution

5.1. Phase-diagram assemblage methodology

The modelling of the petrological evolution has been performed using the phase-diagram calculation software package Perple_X (Connolly, 1990; March 2009 version) and the self-consistent thermodynamic database and mineral solution models of Holland and Powell (1998, with 2002 revision). Amphibole stability relies on Holland and Powell solid solution model (named GlTrTsPg in the program) using White et al. (2003) and Wei et al. (2003) interaction parameters, except for case ZS0833-(2).

Four bulk-rock compositions were used to evaluate the effect of hydrothermal alteration on topology, phase abundances and fluid transfers. Reference sample ZS0833 comes from Lago di Cignana (Valtournanche, Italy; locality 3; Fig. 4f). Sample ZS0716 was sampled in the cliff between Chamois and Buisson (locality 4; Valtournanche, Italy). Bulk-rock compositions of these samples were calculated in the NC(K)FMASH system from modal phase proportions (given under each P–T pseudosection) and average microprobe chemical analyses (representative analyses are given in Appendix A).

Modal phase proportions were estimated by surface ratio calculation on a high-resolution scanned image of the thin sections, using a Matlab program routine. The composition of lawsonite pseudomorphs is estimated using the epidote and paragonite average compositions weighted by their average modal amounts in each sample. Note that our estimated bulk-rock composition for ZS0833-(1) (Table 5) is very close to our ICP-MS bulk-rock analysis, as well as to those of Widmer (1996; XRF analyses) and Groppo et al. (2009; ICP-MS and SEM-EDS analyses) for the same eclogite outcrop on the southern edge of Lago di Cignana. Bulk-rock analyses of a fresh eclogite from Pfulwepass (PVB-941; Bearth and Stern, 1971) and of a pillow rim (BS79; averaged value from four pillow rim compositions from Mattmark and Täschtal areas; Bearth and Stern, 1979) were also used to discuss the effect of ridge-processes on pseudosection topology.

For the P–T pseudosections, water is considered to be in excess and pure. As recalled earlier (Section 2.2), field evidence indeed suggests that free water was available during metamorphism and enabled the crystallization of hydrated phases during eclogite-facies conditions (e.g. hydration of the Allalin gabbro, Chinner and Dixon, 1973; Bucher and Grapes, 2009). We nevertheless studied the influence of variable initial water contents on the peak assemblage of these eclogite-facies metabasalts. Activity of CO_2, which is very low in most of the eclogites, was only considered for the pillow rim pseudosection where carbonates are widespread (BS79).

The variations of modal amounts were calculated along a P–T path following the average path of Angiboust et al. (2009) obtained for the ZS ophiolite. Peak conditions considered here are 550 °C and 24.5 kbar. In order to evaluate independently the effect of increasing the oxygen fugacity on the pseudosection topology, a complementary set of calculations was performed on the rock composition from Lago di Cignana (ZS0833). For all other calculations Fe_2O_3 was neglected because Fe^{3+} content is very low in these eclogites (as in most ZS eclogites, as shown before) and because interaction parameters of riebeckite with other amphiboles are poorly-constrained for HP-LT eclogites (Ballevre et al., 2003 and Warren and Waters, 2006).

Table 5
Inter-study comparison of Lago di Cignana bulk-rock compositions. All analyses were normalized to 100. See text for details.

	Ref. sample method	Groppo et al. (2009)		Widmer (1996)	This study	
		OF2512		V1	ZS0833	
		SEM-EDS	ICP-MS	XRF	Modal calc.	ICP-MS
Normalized bulk composition (wt.%)	SiO_2	51.8	52.8	52.4	51.9	49.8
	Al_2O_3	17.9	16.2	16.4	16.9	17.7
	FeO	9.4	10.3	11.1	9.8	10.3
	MgO	5.6	6.1	6.3	6.2	8.0
	CaO	10.0	9.4	9.1	10.4	10.4
	Na_2O	4.9	4.8	4.5	4.5	3.5
	K_2O	0.3	0.3	0.2	0.4	0.3
	H_2O	–	0.6	0.7	–	0.9

Given that the rocks underwent a progressive chemical fractionation during porphyroblast growth (e.g., Marmo et al., 2002), effective equilibrium compositions may substantially change during each stage of the P–T history (e.g., Konrad-Schmolke et al., 2008). The fact that manganese is mainly concentrated within chemically isolated garnet cores bears two implications: (1) MnO can be neglected in all calculations, (2) in order to better reproduce the P–T evolution from prograde upper BS conditions onwards, the composition of garnet cores was removed from the bulk-rock composition estimate. Note that a possible mismatch between our pseudosections and "ideal" pseudosections obtained through incremental changes of the bulk composition (Konrad-Schmolke et al., 2008) only lies in the prograde portion for pressures <20–22 kbar.

5.2. Predicted phase relationships and the effect of hydrothermal alteration

ZS0833 represents a typical hydrated basalt with an inferred peak assemblage comprising ~1/3 hydrated minerals such as lawsonite (~20 vol.%), glaucophane (>10 vol.%) and phengite (4 vol.%). In order to compare the effect of bulk-rock chemistry and to test the stability of the model, we calculated four P–T pseudosections for classical metabasalts from four different localities on the same P–T range with H_2O-saturated conditions.

5.2.1. The Lago di Cignana eclogite: a typical eclogitized metabasalt

The ZS0833-(1) P–T pseudosection is taken as representative of hydrothermalized basalt in the ZS ophiolite (Fig. 6a). This pseudosection, calculated in the P–T range 10–30 kbar and 400–650 °C, consists mostly of tri- and quadrivariant fields (light and medium grey, respectively, in Fig. 6a). This pseudosection has been calculated minus garnet cores (defined by the Mn-rich domain) to limit the fractionation effect. Blueschist facies assemblage is characterized by the Omp–Law–Gln–Phg–Chl field (Fig. 6a). Entrance in the eclogite-facies field occurs during burial when garnet begins to form at the expanse of chlorite at ~480 °C and ~20 kbar during burial of the rock.

Under peak conditions, the predicted assemblage and the relative vol.% proportions are Omp(46)–Grt(20)–Law(11)–Gln(18)–Phg(4)–Qtz(1) (Figs. 5, 6a, 7a, 8a). The post-eclogitic assemblage is characterized by the progressive growth of glaucophane at the expanse of omphacite. Lawsonite breakdown occurs around 535 °C and 17 kbar and leads to an increase from 35 to 43 vol.% of the glaucophane content (Fig. 7a). Lawsonite breakdown is followed by garnet breakdown (525 °C, 16 kbar). Phase proportions thus change dramatically in the pseudosections (Fig. 7a) in a very narrow range in pressure (15–17 kbar) and temperature (520–530 °C). For the pseudosection shown in Fig. 6a, where the garnet rim is included in the whole-rock composition, lawsonite is pseudomorphed only by

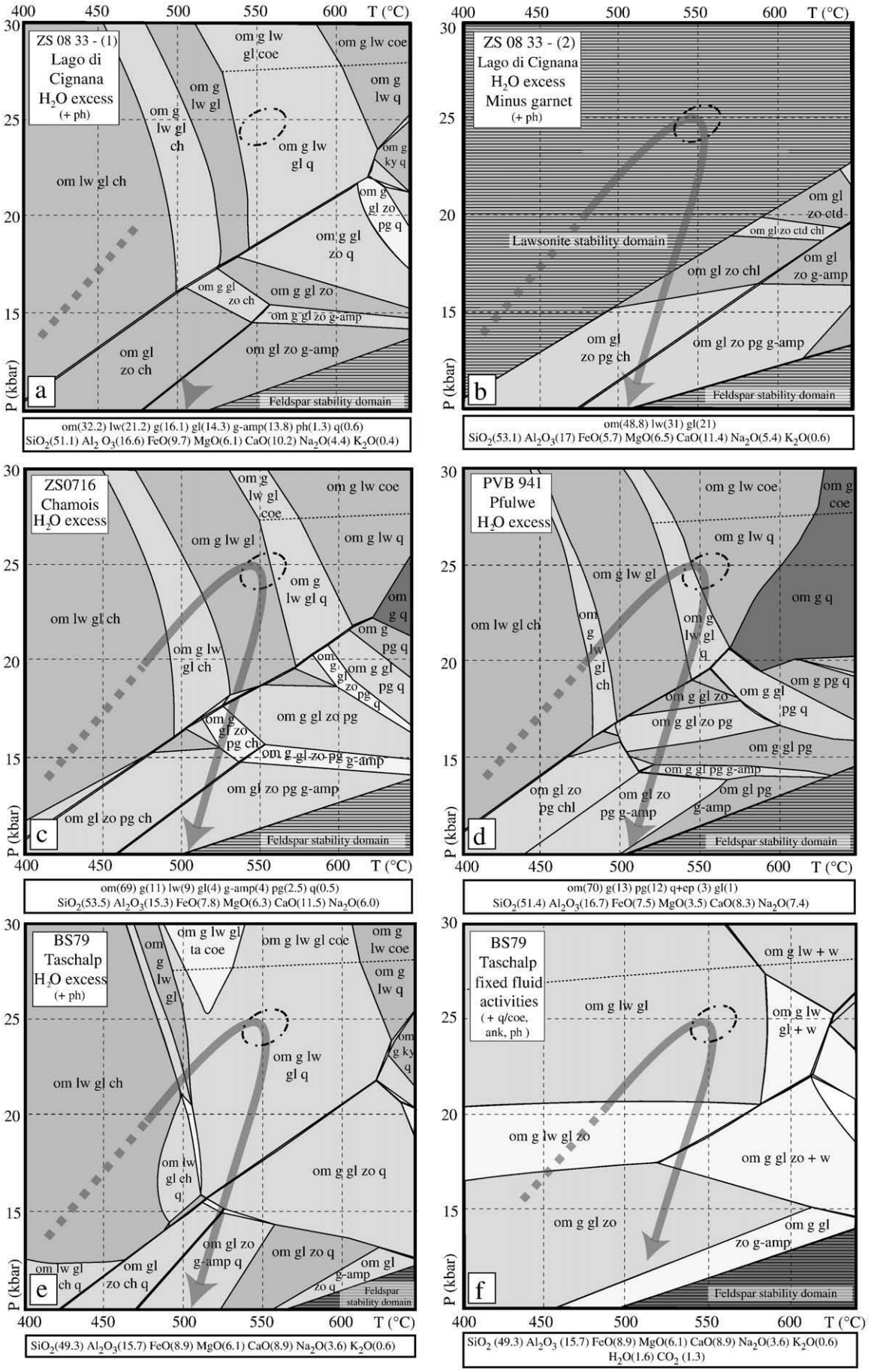

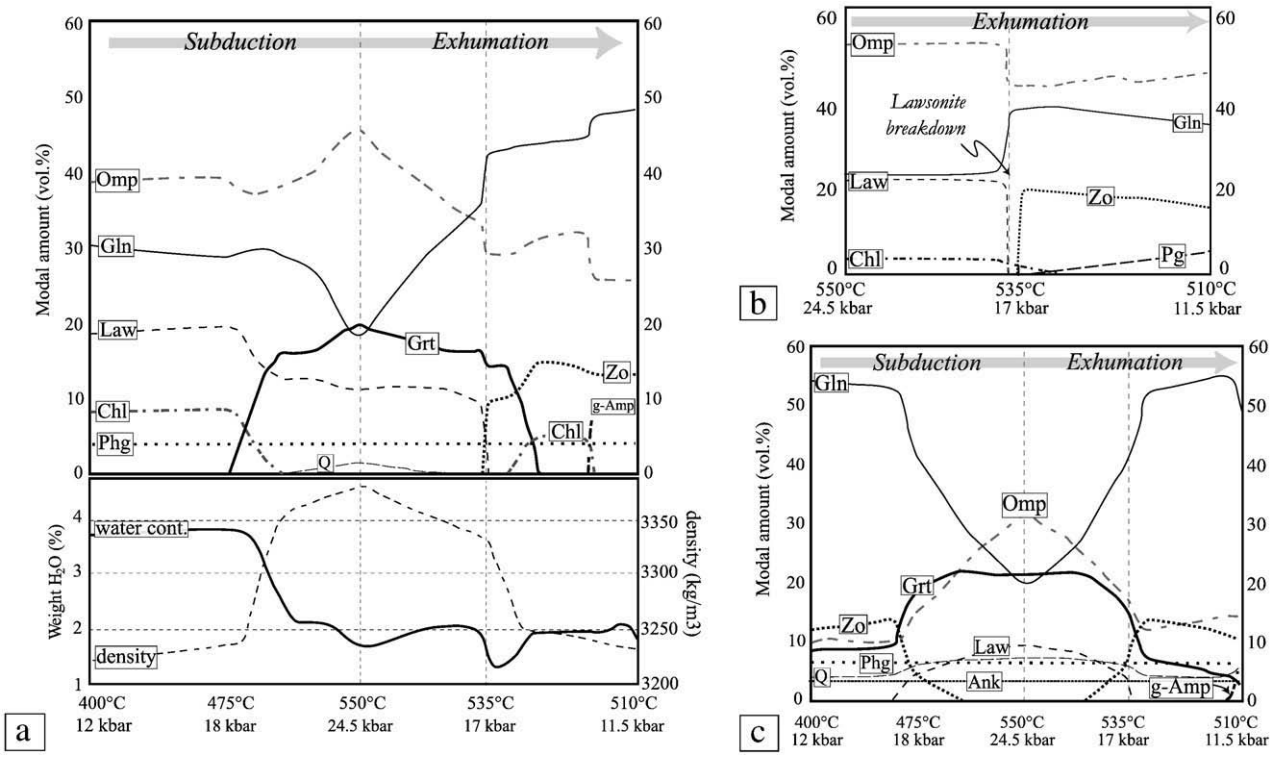

Fig. 7. Calculated phase abundances along the P–T path shown in Fig. 6, represented by the combination of two straight lines from 400 °C/12 kbar to 550 °C/24.5 kbar and from 550 °C/24.5 kbar to 510 °C/11.5 kbar, respectively. a) Phase abundances for the Lago di Cignana ZS0833-(1) eclogite (Fig. 6a). Bottom part of figure: associated variations in water content (black solid line) and densities (dashed line). b) Phase abundances during exhumation in the case of a garnet-free Lago di Cignana eclogite (Fig. 6b) showing the effect of fractional crystallization of garnet on the lawsonite-bearing assemblage in the matrix. c) Simulation for the average of pillow rims (composition BS79; Fig. 6e) with fixed amounts of H_2O (1.6 wt.%) and CO_2 (1.3 wt.%).

epidote. In order to better reproduce the petrological processes in the lawsonite microdomain, a new pseudosection was calculated (Fig. 7b), in which garnet was completely removed (it is in fact well-preserved in most Lago di Cignana eclogites) and only the phases which are susceptible to react with lawsonite were taken into account (Figs. 6b and 7b; i.e., Omp, Law, Gln and Phg). Pseudomorphs after lawsonite predicted by this garnet-free pseudosection are made of 78 vol.% epidote and 22 vol.% lawsonite under 510 °C and 11.5 kbar in lower epidote blueschist facies conditions (Fig. 7b).

5.2.2. Effect of Fe^{3+} content on peak mineral equilibria

Ferric iron content may significantly affect phase relationships during metamorphism (e.g., Diener and Powell, 2010). Assessing ferric iron content under eclogite-facies conditions is difficult, however, because many later metamorphic events can affect the bulk-rock oxidation during exhumation (e.g., Pognante, 1985; Groppo and Castelli, in press).

In order to assess the effect of increasing ferric iron content, we focussed on the reference sample ZS0833-(1). Two reasonable bounds for the bulk rock Fe^{3+} content ($Fe_2O_3 = 0.6\%$ and $Fe_2O_3 = 1.2\%$) were derived from ferric iron content within omphacite (Droop, 1987), glaucophane (Leake et al., 1997) and epidote. The P–T grid ZS0833-(3) with 0.6% Fe_2O_3 (Fig. 9) has been calculated considering that Fe^{3+} is only hosted by omphacite (Green et al., 2007) and epidote (Holland and Powell, 1998), given that analyzed glaucophane and garnet have a low Fe^{3+} content (Table 4). Many similarities with Fig. 6a ($Fe_2O_3 = 0\%$) can be noticed. The main difference is based on the appearance of talc close to peak conditions.

We tested several combinations of distinct activity models for amphibole and garnet in order to evaluate the robustness of our model (see Supplementary material B). Whatever the set of activity models, increasing Fe^{3+} content of the rock implies (i) an increase of the lawsonite content (up to c. 20 vol.%), (ii) the stabilization of talc (up to 9 vol.%) growing at the expense of glaucophane, and (iii) a density decrease (down to c. 3300 kg m^{-3}). The best agreement between observed and calculated phase proportions (Supplementary material B) is obtained for null or low ($Fe_2O_3 = <0.6\%$) ferric iron contents, since talc has never been reported in classical ZS metabasalts.

The apparent contradiction between the extreme scarcity of talc in eclogitized MOR basalts worldwide (e.g., Garcia-Casco et al., 2002; Davis and Whitney, 2006), experimental data (e.g., Forneris and Holloway, 2004) and its high abundance (10–20 vol.%) in recent thermodynamical modelling (e.g., Rebay et al., 2010) raises the question of the compatibility between omphacite, talc, chlorite and recent amphibole models (e.g., Diener et al., 2007) for HP-LT metabasalts.

Fig. 6. Pressure–temperature pseudosections calculated with Perple_X (Connolly, 1990) with excess water (except for f), for four different bulk compositions of MORB-derived metabasalts (shown in Fig. 5). Modal abundances used for bulk-rock composition calculations are given in vol.% and the resulting bulk-rock compositions are in wt.%. The grey-shaded arrow represents the synthetic P–T path for the ZS ophiolite, while the dotted ellipse gives the averaged P–T estimate for peak conditions (Angiboust et al., 2009). White, light grey, low medium grey, high medium grey and dark grey correspond to di-, tri-, quadri-, penta- and hexavariant fields, respectively. Mineral abbreviations: ank (ankerite), ch (chlorite), coe (coesite), g (garnet), g-Amp (green amphibole), gl (glaucophane), ky (kyanite), lw (lawsonite), om (omphacite), pg (paragonite), ph (phengite), ta (talc), q (quartz), w (water), zo (zoisite). a) P–T pseudosection for a typical, strongly hydrated metabasalt from Lago di Cignana (ZS 08 33-(1); locality 3). b) P–T pseudosection for the same Lago di Cignana sample, considering only matrix phases subject to reaction during lawsonite breakdown (i.e., omp, gln and law) and thus removing the garnets. c) P–T pseudosection for a representative, slightly hydrated bulk composition from locality 4 (Valtournanche). d) P–T pseudosection for a paragonite-bearing metabasalt from Bearth (1973) from Pfulwepass locality. e) P–T pseudosection for an average of pillow rim compositions (from Bearth and Stern, 1979). f) Same composition as e) with fixed amounts of H_2O and CO_2.

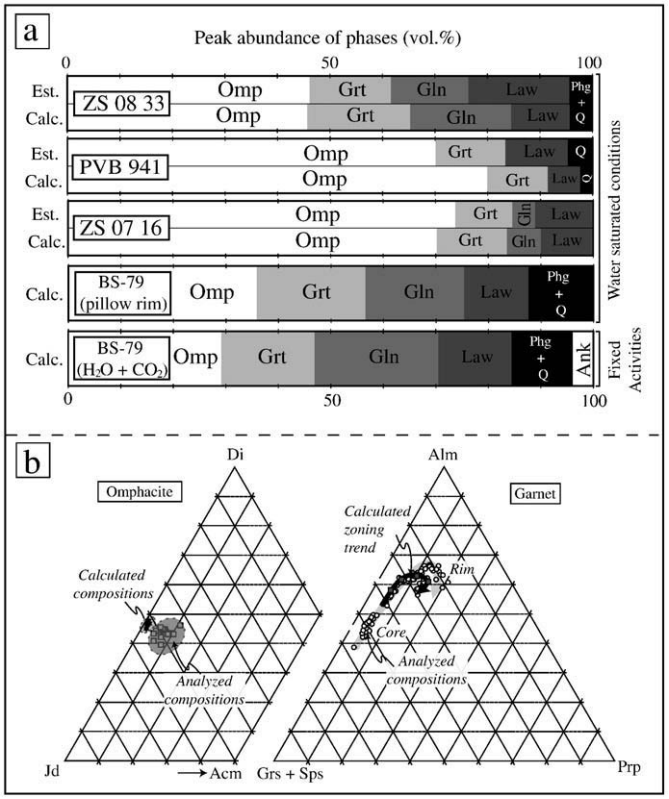

Fig. 8. a) Comparison between inferred visual estimates (Est., up) and calculations (Calc., bottom) of modal phase abundances for the P–T pseudosections of Fig. 6 under peak conditions (550 °C, 24.5 kbar). Inferred compositions were calculated assuming that green amphibole formed equally from omphacite and glaucophane, that half of the glaucophane content comes from omphacite and that paragonite formed after lawsonite. Mineral abbreviations as for Figs. 6 and 7. b) Comparison between microprobe analyses from the ZS0833 eclogite and compositions derived from Perple_X along the burial P–T path of Fig. 6 for omphacites (left) and for a garnet core to rim transect (right). Garnet and pyroxene end-members: Acm: acmite; Alm: almandine; Di diopside; Grs + Sps: grossular + spessartine; Jd: jadeite; Prp: pyrope.

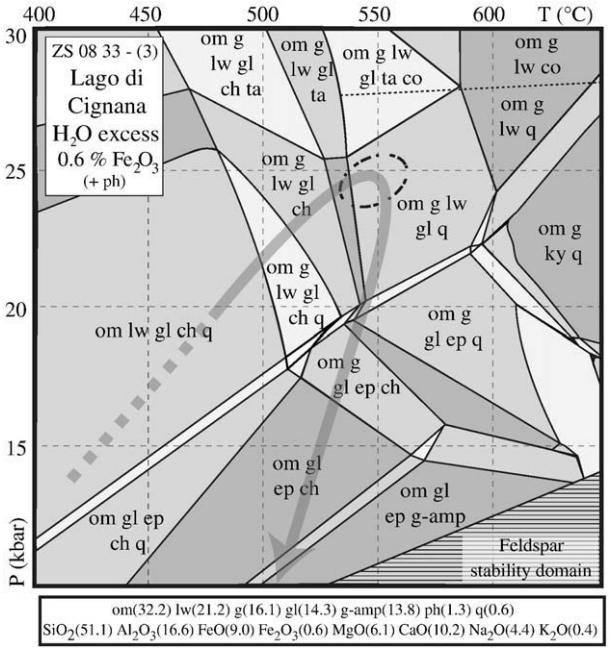

Fig. 9. P–T pseudosection calculated on L. di Cignana eclogite composition ZS0833-(3) considering an average Fe^{3+} content (see Fig. 6a for comparison). Abbreviations are similar to Fig. 6 except for ep: epidote.

5.2.3. Effects of variable bulk-rock chemistry on phase-diagram topology

Sample ZS0716 (Fig. 6c) has a bulk-rock composition relatively enriched in Na_2O compared to ZS0833 (Fig. 5). Under peak conditions, the assemblage composition and relative proportions are Omp(70)–Grt(13)–Gln(10)–Law(7). The exhumation pattern is similar with the formation of glaucophane at the expanse of omphacite and garnet and zoisite and paragonite ± chlorite at the expanse of lawsonite.

Sample PVB 941 (Fig. 6d) is characterized by a relatively high content in Na_2O (7.4 wt.%) and a relatively low content in MgO (3.5 wt.%; Fig. 5). All the glaucophane present in the blueschist facies assemblage has been consumed by omphacite and garnet during eclogitization of the rock. The peak assemblage and relative proportions of species for this pseudosection are Omp(80)–Grt(15)–Law(3)–Q(2). After lawsonite breakdown, the stable assemblage is Omp–Grt–Gln ± Zo ± Pg.

Sample BS79 (Fig. 6e) has a bulk composition very close to that of ZS0833 (Fig. 5). Even if the slight differences in whole-rock composition led to apparently different topologies, the relative proportion of phases under peak conditions are similar (Figs. 5 and 8a).

5.2.4. Pillow zonation and effect of adding CO_2 on phase abundances

Carbonates are widespread in the Täschalp area, within eclogitized pillows rims (Fig. 3c), and are associated with garnet, glaucophane, phengite, epidote, omphacite and lawsonite (Bearth, 1967; Oberhansli, 1982; Barnicoat, 1988). In P–T pseudosection BS79, the topology is deeply modified by the presence of a high CO_2 content (Fig. 6f). The average value of CO_2 content (1.3 wt.%; H_2O is 1.6 wt.%, for comparison) taken from Bearth and Stern (1979) analyses falls within the broad range reported by Alt and Honnorez (1984) for variably altered sea-floor basalts. The main modifications in topology are (i) stabilization of garnet towards blueschist facies conditions, (ii) stabilization of a Ca–Fe–Mg carbonate (ankerite) on the entire grid, (iii) stabilization of zoisite up to 21 kbar in the lawsonite stability field and (iv) much higher amounts of glaucophane under epidote blueschist facies conditions (>50 vol.%) (Fig. 7c). Lawsonite abundance under peak conditions remains comparable to estimates from previous P-T grids (Fig. 8a).

5.2.5. Effect of initial water budget on peak conditions modal abundances

We evaluated the effect of lowering the initial water budget of the rock (Fig. 10). Decreasing initial water content systematically implies the expansion of eclogite-facies minerals (grt + omp) at the expanse of glaucophane and lawsonite. Comparison of these diagrams with estimated peak modal abundances reveals that the best fit between modelled data and petrological observations is obtained for high initial water contents, close to saturation, whatever the bulk-chemistry (grey-shaded area, Fig. 10a, b, c). Rock "dehydration" is accompanied by a progressive increase in density mainly driven by the increase in garnet content. While densities range from 3300 to 3420 kg/m^3 for strongly hydrated parageneses (see Section 6.3), dry eclogites with the same bulk composition have densities between 3440 and 3500 kg/m^3.

6. Discussion

6.1. Detailed tracking of the mineralogical evolution

Petrological observations and pseudosection modelling indicate that burial is characterized by the blueschist facies assemblage Omp + Gln + Law + Chl ± Phg. Blueschist–eclogite transition assemblages are preserved as inclusions (mainly glaucophane and lawsonite) in garnet cores within the Mn-rich domain. Glaucophane amounts

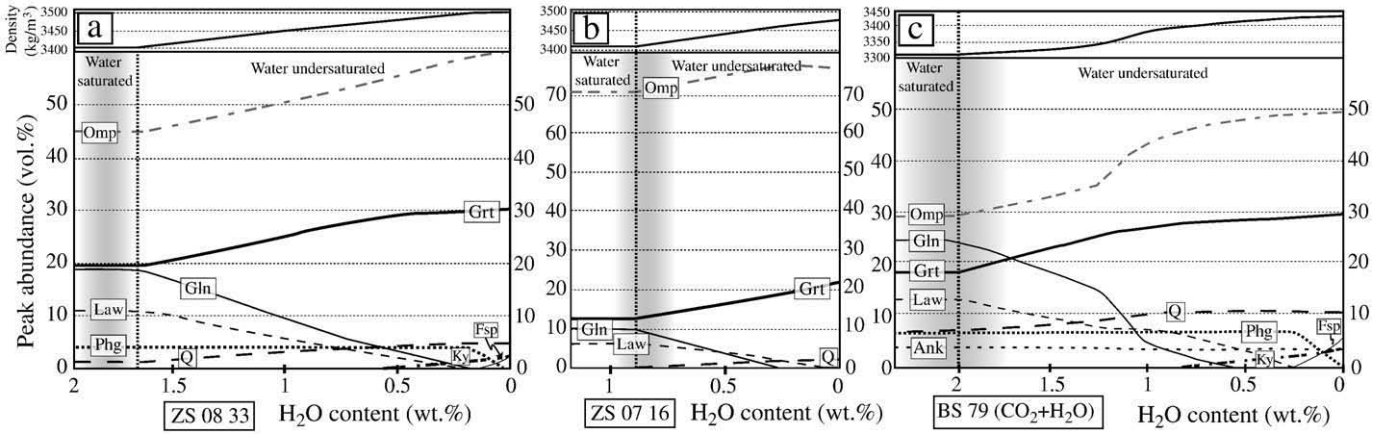

Fig. 10. a–c) Effect of water availability on the modal phase abundances under peak conditions: phase abundances were calculated for different H_2O contents by steps of 0.1 wt.% increments. Mineral abbreviations as for Figs. 6 and 7. The grey-shaded area corresponds to water amounts for which calculated phase abundances best match those estimated for the original eclogitic rock. These calculations evidence that water-saturated, or close to water-saturated conditions prevailed at peak conditions in the ZS ophiolite. The evolution of densities as a function of the water content is also shown, for each sample, in the top inset.

decrease in the metabasalt at the expanse of omphacite between 20 and 24.5 kbar to reach 20 vol.% under peak conditions.

Coeval omphacite and garnet growth in eclogite facies is predicted for the reference pseudosection ZS0833 between 480 °C/20 kbar and 550 °C/24.5 kbar. Other pseudosections allow evaluating its sensitivity to changing chemical compositions (Fig. 6). As CaO, FeO, MgO partition between glaucophane, garnet and omphacite, evaluating independently the effect of varying one of them on the system topology is impossible. However, even if the boundaries and the field dimensions change from one composition to the other, the overall pattern for the classical metabasalts is very similar and shows: (i) a consumption of glaucophane at the expanse of garnet and omphacite during eclogitization (Fig. 7a), (ii) relatively constant amount of garnet under peak conditions (Figs. 7a and 8a), and (iii) stability of lawsonite during burial and early exhumation (Fig. 7a). The main differences are essentially the variations in omphacite (36–80 vol.%) and glaucophane (0–18 vol.%) abundances under peak conditions (Fig. 8a).

In sample ZS0716, modal abundances under peak conditions are characterized by the pre-eminence of omphacite (70 vol.%) and match observed abundances (Fig. 8a). This also holds true for sample PVB941 where pseudosection modelling predicts that 92 vol.% of the rock is made of omphacite and garnet under peak conditions, in agreement with rock mineralogy. Paragonite, fairly abundant in this sample (12 vol.%), is thought to form from the reaction between omphacite and lawsonite during retrogression.

Calculated phase compositions too are very similar to those analyzed (Fig. 8b). As discussed previously, the absence of Fe^{3+} in most of our pseudosections may account for the slight shift between our microprobe analyses and predicted omphacite compositions. The garnet zoning trend with increasing almandine content followed by pyrope enrichment is well reproduced. However, modelled peak compositions have slightly (5–10%) lower pyrope content than analyzed garnet rims. This slight mismatch may result from (i) fractionation of magnesium in the matrix during garnet growth, thus creating a disequilibrium between the estimated rock composition and the actual rock volume subject to reaction, (ii) removal of Mn or Fe^{3+} from calculation, (iii) uncertainties related to activity models, and (iv) underestimation of peak conditions of Lago di Cignana eclogites (see previous discussion in Section 2.1).

We emphasize that lawsonite is systematically stable under peak conditions together with garnet–omphacite ± glaucophane. This result is also supported by numerous petrological observations such as lawsonite inclusions within garnet and omphacite cores and rims (Figs. 3f, 4) and dismisses the possibility of a lawsonite-free peak assemblage. Zoisite/paragonite intergrowths (±chlorite) are predicted to form in a 4:1 ratio after lawsonite breakdown in all the samples (e.g., Fig. 7b), which concurs with petrological observations (Fig. 4e–g).

6.2. Water budget and fluid release

6.2.1. Water budget and lawsonite content

In order to further evaluate the amount of water present in the ZS rocks, phase abundances were calculated for various water saturation values (Fig. 10). In order to match calculations and petrological data, Fig. 10 shows that the ZS metabasalts must have witnessed water-saturated conditions under peak conditions. Water-saturated conditions are also supported by strongly hydrated peak assemblages reported in the Allalin gabbro (Chinner and Dixon, 1973; Bucher and Grapes, 2009).

Using our reference ZS0833-(1) pseudosection, we then calculated the evolution of its water content throughout the P–T evolution (Fig. 11a; initial content ~4.5 wt.% under saturated conditions). Given the moderate to high intensity of hydrothermal alteration in the Lago di Cignana eclogites, we assume that 20% of initial water is released during early subduction (mostly through destabilization of clays and zeolites; Peacock, 1993). Once this first dehydration stage is over, the water budget of metabasalts remains relatively constant during subduction under blueschist facies conditions (~3.8 wt.% H_2O). Almost half of the initial water content later escapes from the rock through chlorite destabilization as the rock enters the eclogite facies. Under peak conditions the ZS0833-(1) pseudosection predicts that the Lago di Cignana eclogites contain 11 vol.% lawsonite, with an overall water content of 1.7 vol.%. One should keep in mind that the above amounts of lawsonite and water content in fact correspond to minimum values (Fig. 9), since they may increase in rock domains with higher Fe^{3+} activities (Supplementary material B).

About one third of the initial water content (~35%) is thus preserved at peak conditions, mainly bound in lawsonite and to a lesser extent in glaucophane and phengite. Since lawsonite contains 12 wt.% water and lawsonite pseudomorphs around 4 wt.%, much water is lost during lawsonite breakdown through the reaction:

$$\text{Jadeite} + \text{Lawsonite} = \text{Zoisite} + \text{Paragonite} + \text{Quartz} + H_2O.$$

With a rock containing 11 vol.% of lawsonite, about 0.9 wt.% of total water is lost at this stage. Three contrasting situations can occur however (Fig. 11a): (1) water escapes from the rock, which would then contain 0.8 wt.% water (i.e., ~15% of the initial water content),

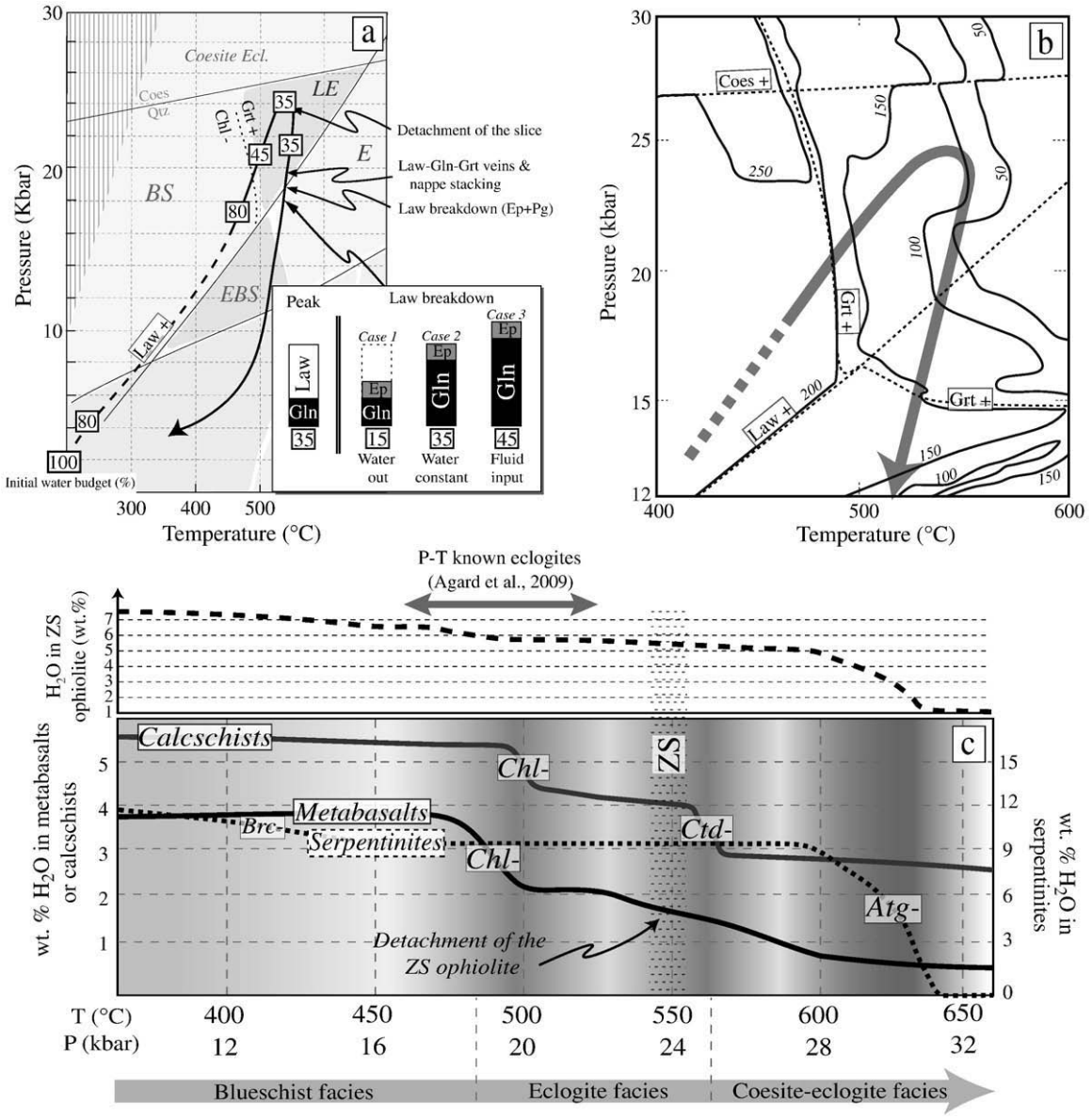

Fig. 11. a) Evolution of the water budget during subduction and exhumation of a hydrothermalized ZS eclogite. Water contents (given as % of the initial water budget) correspond to those estimated by pseudosection modelling on the Lago di Cignana eclogite (ZS0833-(1) — Fig. 6a). Background: main metamorphic facies, as for Fig. 1d. When lawsonite breakdown takes place, three different possibilities are considered: water is lost, internally buffered or gained. See text (Section 6.2.1) for details. b) P–T grid showing the density difference between the hydrated ZS0833-(1) eclogite and a typical "dry" MORB composition (with 0.5 wt.% H_2O; from Hacker et al., 2003a). The hydrated eclogite is buoyant with respect to a standard MORB throughout this whole P–T range (contours are in kg m^{-3}). Garnet growth is the main contribution to density increase in these rocks. c) Evolution of the water content along the burial path recalled in Fig. 11b in the various lithologies of the ZS oceanic lithosphere (left axis: metabasalts and calcschists; right axis: serpentinites). Top curve: cumulative amount of water bound within minerals of the ZS ophiolite considering 50 vol.% serpentinite, 40 vol.% metabasalts and 10% calcschists. Also shown is the range of peak P–T conditions for oceanic eclogites from the compilation in Agard et al. (2009).

(2) water is taken up by glaucophane (the water content is buffered to ~35%), or (3) additional water is added to the rock, allowing for the crystallization of more glaucophane (potentially increasing the water content to ~45 vol.%; as predicted in Figs. 6a and 7a). Average H_2O content (~0.8 wt.%) in Lago di Cignana eclogites (Table 5) supports the first option for these rocks.

Field observations show that pseudomorphs after lawsonite are not systematically associated with retrograde glaucophane (some lawsonite eclogites have very low glaucophane content) and that many blueschist facies shear zones cross-cut eclogitic bodies. Lawsonite content, in the particularly well-preserved Mellichen slice (Fig. 2 III), was not equally distributed either. Lawsonite-bearing veins cross-cutting the main eclogitic foliation and the increase in lawsonite size and abundance on the edges of the slice suggest that (i) these veins and fractures formed in the lawsonite stability field during early exhumation and that (ii) channelized fluid flow and dynamic recrystallization between the slices may have contributed to the massive crystallization of lawsonite along the slices. All this suggests that fluid transfer takes place at scales>m, in addition to cm-scale mineral buffers. Such fluid circulation may in fact be essential for the individualisation, in the ophiolite, of denser mafic bodies surrounded by a mechanically softer and buoyant matrix (see discussion later).

6.2.2. Fluid release at depth

Fig. 11b highlights reactions controlling fluid release in mafic protolith (ZS0833), but also in the surrounding serpentinized peridotites and subordinate calcschists (pseudosections, not shown here, are available on request). Based on surface exposures, the ZS

ophiolite is in first approximation made of a 1:9:10 ratio of sedimentary, mafic and ultramafic protoliths from which allow calculating a bulk dehydration curve (Fig. 11c).

When comparing these dehydration steps with the depth range of oceanic lithospheric pieces returned from subduction zones worldwide (Agard et al., 2009) only the chlorite (and possibly chloritoid) breakdown reactions match (Fig. 11c). Destabilization of chlorite in blueschist facies metabasalts and metasediments may release significant amounts of water at depths of 50–60 km, while sediments will loose some more water through chloritoid breakdown somewhat deeper, at 70–80 km (Fig. 11c). By contrast antigorite breakdown takes place much deeper (Fig. 11c). This is consistent with the results of Scambelluri et al. (1995), Li et al. (2004) and Auzende et al. (2006) demonstrating that the W. Alps serpentinites still contain stable antigorite under eclogite-facies conditions. Antigorite breakdown will release significant amounts of fluids in the mantle wedge (e.g., Iwamori, 1998), yet this will happen at ~100 km (630–675 °C/30–34 kbar, for a cold, 4–8 °C/km geothermal gradient as for the W. Alps; Ulmer and Trommsdorff, 1995), i.e., 20–25 km deeper than the maximum depth reached by the ZS ophiolite.

Importantly, we emphasize that the depths of major fluid release through the prograde chlorite and retrograde lawsonite breakdown reactions broadly coincide, at 50–60 km. Even if a fraction of these fluids may be reabsorbed by adjacent under-saturated rocks, this massive fluid liberation may significantly contribute to the serpentinization of the plates interface. As an example, chlorite breakdown in the oceanic crust (with 100 m sediments and 400 m of hydrothermalized basalts) would alone cause 8 wt.% serpentinization of 1 km^3 of dry mantle in a closed system. These results are consistent with recent geophysical data. While dehydration reactions in the subducting slab are assumed to cause ~20–30% serpentinization of the mantle wedge in the range 20–60 km (Peacock and Hyndman, 1999; Hyndman and Peacock; 2003; Chou et al., 2009), recent seismological observations point to discontinuous and fragmentary serpentinization (Seno, 2005; Xia et al., 2008) and emphasize fluid percolation beyond maximum depths of the seismogenic zone (i.e., 45–60 km; Audet et al., 2009). Note that an intense serpentinization of the mantle wedge will also tend to widen the subduction channel, which may in turn promote exhumation (Raimbourg et al., 2007) and therefore partly account for the sampling of HP-LT rocks from this depth range (Agard et al., 2009).

6.3. Evolution of densities (and viscosities) as a function of water content

6.3.1. Evaluation of buoyancy contrasts

Based on ZS rocks or on a worldwide compilation, Bucher et al. (2005) and Agard et al. (2009) concluded that there are maximum depths (20–23 kbar on average) beyond which the oceanic lithosphere is too negatively buoyant and irreversibly sinks into the mantle. Hence, beyond such depths, the densification of mafic material resulting from eclogitization is not counterbalanced by associated, light serpentinized peridotites. Buoyancy is indeed considered by many authors (e.g., Platt, 1993; Rubatto and Hermann, 2001) as the main effective force able to return deeply subducted rocks to the base of the crust.

Strong initial hydration of the ZS ophiolite (i) enhanced the amount of hydrated phases such as lawsonite and glaucophane during the burial of oceanic crust, (ii) induced a density decrease under peak conditions as less dense hydrated phases (e.g., lawsonite: 3126 kg m^{-3}; glaucophane: 3139 kg m^{-3}) crystallized instead of the dense typical eclogitic phases (garnet: 4060 kg m^{-3}; omphacite: 3358 kg m^{-3}), and (iii) weakened the rock and decreased its viscosity.

The density difference between a water-saturated hydrated metabasalt (ZS0833) and a typical water under-saturated MORB composition is shown in Fig. 11b. The MORB is ~120 kg m^{-3} denser under peak conditions that the hydrated metabasalt (3510 and 3390 kg m^{-3}, respectively). This difference reaches ~250 kg m^{-3} in garnet–lawsonite glaucophanites (magnesian metabasalts) or in more oxidized portions of the rock (Supplementary material B). When taking into account metasediments in each slice, the average density of the slice is strongly lowered and ranges from ~3150 kg m^{-3} for sediment-rich slices (e.g. Courquet slice; Table 1) to 3350 kg m^{-3} for mainly-basaltic slices (e.g. Pfulwe slice). For ZS gabbros (e.g., flaser-gabbros mainly composed of clinopyroxene in a strongly sheared and flattened epidote-rich matrix; Ayas slice, Fig. 2 Ib; Plan Frei slice, Fig. 2 IIb) we obtained an average peak density of 3287 kg m^{-3} using the spreadsheet of Hacker and Abers (2004).

To evaluate the buoyancy of these ZS eclogitized slices with respect to surrounding mantle rocks on either sides of the channel (taken here as moderately hydrated: i.e., 30 wt.%, based on mantle wedge estimates), one needs to combine densities of the mafic parts (Table 1) and densities of their associated fraction of highly serpentinized (i.e., 90 wt.%) slab mantle. Computated densities are ~2880 kg m^{-3} for a completely serpentinized mantle and ~3330 kg m^{-3} for a dry mantle.

Fig. 12 shows, for contrasting densities of mafic bodies, the fraction of serpentinized mantle required to produce a tectonic slice lighter than a 30% serpentinized mantle ($\rho = 3091$ kg m^{-3}). For the range of densities of the ZS mafic bodies, Fig. 12 shows that the ratio of ultramafic/mafic material should be greater than 1 (which corresponds to the ratio deduced from outcrop exposures; Fig. 2). This plot also shows that the buoyancy contrast at peak conditions between the slices and the surrounding mantle will be relatively small (between -50 and $+100$ kg m^{-3}).

6.3.2. Upward migration after detachment

Once detached, the upward migration of a (ZS ophiolite) tectonic slice will linearly depend on the following ratio: $(\rho_s - \rho_m)/\eta$, where $(\rho_s - \rho_m)$ represents its density contrast and η represents the viscosity of the surrounding matrix/mantle. This dependency comes from the Stokes equation, as used by Schwartz et al. (2001), and is also found in the exhumation number proposed by Raimbourg et al. (2007). In contrast to the densities discussed previously, the evolution of the viscosity as a function of the P–T conditions is unknown.

Application of the Stokes equation allows in principle to calculate the minimum velocity of a sphere in a weak viscous environment. The average ZS ophiolite slice is 300 m × 2000 m × 3000 m and would correspond to a sphere radius of 750 m, yet a spherical shape may not be very valid since eclogitic lenses are lenticular and flattened (Figs. 2 and 3): flattening will further decrease velocities through enhanced friction, whereas a lenticular shape may prove more efficient to move along the subduction channel, but whether these two effects cancel out is unclear.

Considering a rather low density contrast ($\Delta\rho = 50$ kg m^{-3}; Fig. 12) between the ZS ophiolite and the surrounding serpentinized mantle present on either sides of the channel, we obtain velocities of 20 m My^{-1}. Note that we chose $\eta = 10^{20}$ Pa s^{-1}, which in fact corresponds to 50% serpentinized mantle (Schwartz et al., 2001), since heterogeneous serpentinization along fractures will result in an overall effective viscosity trending towards that of fractures (Escartin et al., 2001). This velocity is nevertheless one or two orders of magnitude lower than the 2 cm yr^{-1} obtained by Amato et al. (1999) for L. di Cignana. To match such velocities, viscosities of 10^{17} are required, which is not realistic according to recent measurements (Hilairet et al., 2007). These simple calculations suggest that buoyancy contrasts alone cannot account for the exhumation of the ZS rocks.

6.4. Implications on exhumation and fluid processes in the subduction channel

We herein propose a tentative model evolution for the ZS ophiolite and discuss how this sheds light on subduction channel processes (Fig. 13). We propose that the various slices recognized here derive, as

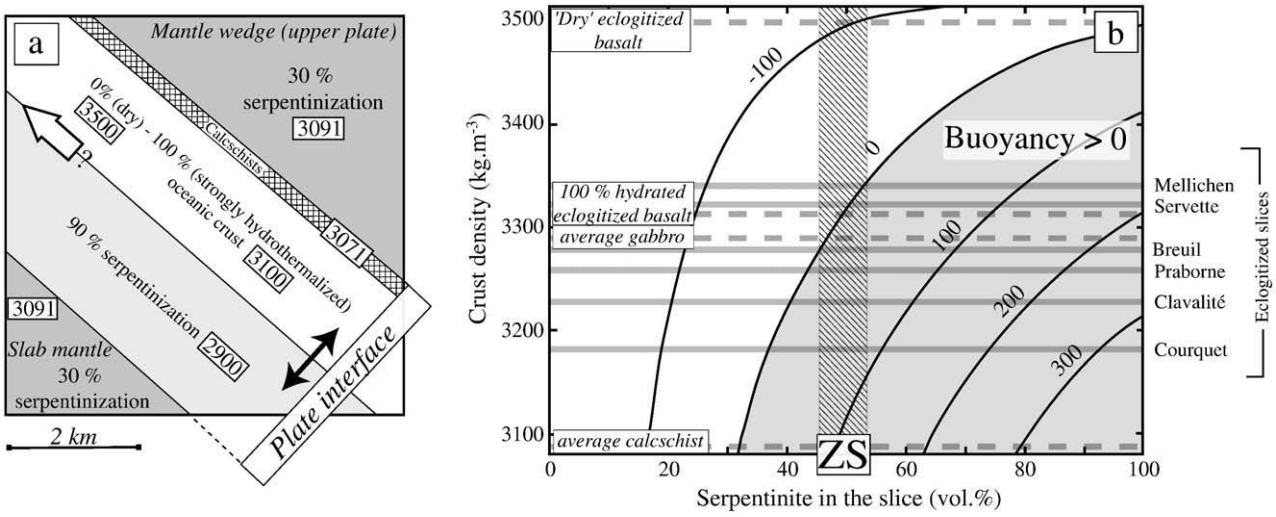

Fig. 12. a) Idealized, schematic view of a tectonic slice of oceanic lithosphere (whose buoyancy is evaluated in b) possibly ascending along the subduction channel. b) Grid showing the density difference under peak conditions (550 °C, 24.5 kbar) between a tectonic slice, as shown in (a), and the surrounding mantle (moderately hydrothermalized; i.e., 30%). The tectonic slice can be thought of as being made of variably hydrothermalized crust with contrasting densities (y-axis of figure; dotted lines: densities of a dry or fully hydrated metabasalt, and of an average gabbro and calcschist) and of various proportions of highly hydrothermalized mantle (x-axis). The grey field underlines the conditions which favor exhumation (buoyancy >0). Densities of the crustal part of the various ZS tectonic slices (see Table 1 for mafic/sedimentary proportions and exact densities) are recalled as grey lines. They suggest that a minimum mantle:crust ratio of 1:1 (i.e., 50 vol.% serpentinite in slice) is required to ensure the buoyancy of the ZS slices (note that, in comparison, almost 100% of serpentinite would be required for a dry metabasalt). Mantle density was computed using an average ZS harzburgite composition from Li et al. (2004): SiO_2(40), Al_2O_3(1.9), FeO (7.2), MgO(38.7), CaO(0.6), and H_2O(10.2).

a first approximation, from a coherent tectonic unit, with possibly slight density differences depending on the degree of hydrothermal alteration and on the relative proportions of metasediments (Figs. 12b and 13a). This is supported by (i) very similar P–T conditions across the slices (and peak temperature conditions in associated metasediments; Angiboust et al., 2009), (ii) numerous occurrences of preserved, undisturbed basalt-sediment contacts, and (iii) occurrences of serpentinite slivers strictly restricted to shear zones between the slices.

This huge body detached from the sinking slab at depths of 70–80 km (23–25 kbar) and was later sliced up on exhumation, under fluid present, blueschist facies conditions at 17–18 kbar (Fig. 13b,c). The formation of several slivers amounting to ~2–3 km thick is in agreement with inferred subduction channel widths (Abers et al. 2006; Hilairet and Reynard, 2009).

The ZS ophiolite was returned along the subduction channel at rates (2 cm yr^{-1}; Amato et al., 1999) which cannot be accounted for by buoyancy contrasts alone (as shown in the previous paragraph). These rates were possibly enhanced by internal subduction channel dynamics (e.g., Schwartz et al., 2001; Gerya and Stöckhert, 2002; Guillot et al., 2009). The scarcity of very dense oceanic eclogites exhumed along subduction zones (see the compilation by Agard et al., 2009), shows, however, that density contrasts dominate over subduction channel dynamics and effectively prevent their upward migration along the subduction plane. The fast return of the ZS ophiolite was therefore likely assisted, from blueschist facies conditions onwards, by the rise of an adjacent, much more buoyant material (i.e., the continental material from the Mt Rosa internal massif; Lapen et al., 2007; Fig. 13d).

We envisage that enhanced mechanical coupling (Fig. 13b) and/or large earthquakes (as for Sumatra earthquake in 2004: Singh et al., 2008; Chile earthquake in 2010), possibly reworking shear zones in the strongly hydrated crust and/or serpentinized slab mantle, were responsible for the detachment of this large tectonic slice. Strong hydration of the ZS ophiolite is responsible for a higher buoyancy and for a weakening of the material, through a decrease in viscosity (although this cannot be quantified) and repeated microfracturing (e.g., Fry and Barnicoat, 1987). Enhanced buoyancy prevented the ZS ophiolite from irreversibly sinking into the mantle. We also propose that its significantly higher water content enabled the detachment of a much larger ophiolite sliver with more mafic material than that of the nearby Monviso.

Finally, we predict through thermodynamic modelling a domain of strong hydration at 50–60 km in the subduction channel, associated with chlorite and lawsonite breakdown (with the possible addition of deeper fluids from antigorite breakdown). We underline that these depths where fluid is most abundant correspond to depths at which episodic tremor slip was recently described (Rogers and Dragert, 2003; Audet et al., 2009) and to common depths at which tectonics stacking takes place in the W. Alps (i.e., 15–18 kbar). These conclusions are also in line with the growing recognition of the key role played by fluids in subduction zones (hydrated serpentinized mantle wedge: Guillot et al., 2001; Hyndman and Peacock, 2003; link between dehydration reactions and double seismic zones: Hacker et al., 2003a,b).

7. Conclusions

The Zermatt–Saas ophiolite corresponds to the largest exhumed body of lawsonite eclogite and the deepest fragment of oceanic lithosphere returned from a subduction zone worldwide and provides key insights into subduction channel processes.

Field observations reveal that the ZS ophiolite is made of a stack of highly hydrothermalized mafic tectonic slices several 100 m thick, interleaved with serpentinites. A thick, strongly serpentinized mantle sole is also found at the base of these slices. The initial water input, during MOR hydrothermal alteration, favored the crystallization under eclogitic conditions of lighter, hydrated minerals (glaucophane, lawsonite) than those found in common eclogitic assemblages (garnet, omphacite). Our investigations suggest that water remained in excess from burial to eclogitic peak conditions and that eclogite densities of the various ZS slices were at least 100 to 250 kg m^{-3} lighter than those of usual dry eclogites.

We thus propose that the unusually large dimensions of the eclogitic ZS ophiolite (with respect to nearby ophiolite bodies such as Monviso, for example) mainly result from its initial strong hydration.

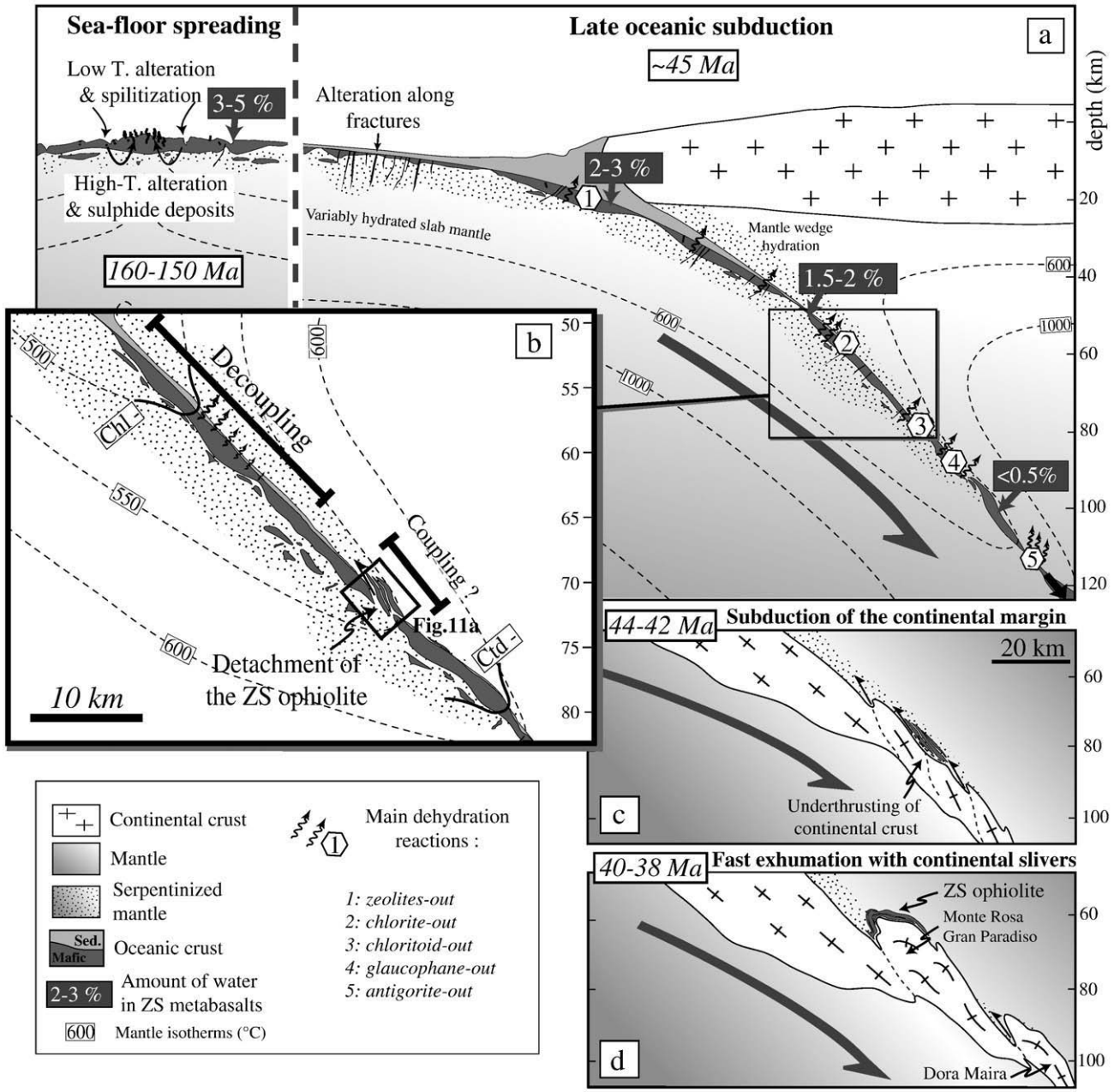

Fig. 13. a) Synthetic overview of the evolution of ZS ophiolite from water enrichment (in particular during early stages of seafloor spreading) to fluid release during burial. Water content is given in wt.%. See text for details. b) Inset emphasizing the conditions prevailing at depth during the detachment of the ZS ophiolite. Major reactions involving fluid liberation are recalled. Strong hydration of the ZS ophiolite was responsible for its enhanced buoyancy (which prevented the ZS ophiolite from irreversibly sinking into the mantle and allowed the exhumation of a large ophiolite sliver with significant mafic material; see Fig. 12b) and for a weakening of the material. Large earthquakes were probably responsible for the detachment of this large tectonic slice. c–d) Final return of this ZS ophiolite was triggered/assisted by the underthrusting of much more buoyant material (i.e., the Monte Rosa and Gran Paradiso Internal crystalline massifs) during continental subduction.

The hydration was both responsible for its enhanced buoyancy, which prevented it from irreversibly sinking into the mantle, and for a significant weakening of the material.

Simple calculations suggest, however, that the density contrast between these tectonic slices (mafic and ultramafic in a 1:1 proportion, approximately) and the surrounding variably hydrated mantle was probably only moderate and yield exhumation velocities smaller than those reported (e.g., Amato et al., 1999). The relatively fast exhumation of the ZS slices, which were probably detached along the subduction channel by large earthquakes, was finally assisted by the exhumation of the buoyant underlying continental units of the nearby internal crystalline massifs (as suggested, for example, by Lapen et al., 2007; Agard et al., 2009).

Acknowledgments

We would like to thank Silvana Martin for sharing her knowledge of the St-Marcel Area, and Loic Labrousse and Benjamin Huet for comments and discussions. Two anonymous reviewers are thanked for helpful and thoughtful comments. Christian Chopin is thanked for allowing us to perform complementary analyses with the Raman Spectrometer and Hubert Whitechurch for providing us with the ICP-MS analyses. René Boutin, Michel Fialin, Fréderic Couffignal, Didier Devaux, Abdeltif Lahfid and Marco Moroni are thanked for their technical assistance. The authors would also like to acknowledge the Syndic of Fenis and the National Park of Mont Avic (particularly M. Bocca) for technical assistance on the field. Fieldwork and analyses

were funded through two projects obtained by P. Agard: Egide-PHC Alliance 19349F and INSU Syster. Additional support from the ISTeP group 'Lithosphere et Processus Profonds' is greatly acknowledged.

Appendix A. Analytical methods

Major element analyses of nine eclogitized metabasalts (Table 3) were analyzed at Ecole et Observatoire des Sciences de la Terre in Strasbourg, France. An aliquot of each sample was crushed and powdered for 20 min with an electric mortar in agate to avoid contamination. About 1 g of sample was dried at 110 °C and heated to 1000 °C for 3 h for chemical preparation. A 100 mg fraction of each sample was then mixed with 750 mg lithium tetraborate in a vitreous graphite crucible and fused at 1000 °C in a silica muffle furnace under an atmospheric pressure of argon for 30 min. After cooling, the glass was directly dissolved in the crucible containing dilute nitric acid and glycerine. The final dilution was 4 g/dm^3 (100 mg of sample in 25 ml solution). After filtering, the 4 g/dm^3 solution was analyzed by ICP-AES. The same solution was diluted 10 times for analysis by ICP-MS. Calibration curves were prepared using five solutions: a blank (750 mg lithium tetraborate which was fused and dissolved in dilute nitric acid and glycerine) and four CRPG reference materials: AN-G, BEN, GS-N and VS-N. Four other standards were analyzed every six samples in order to monitor the possible drift of the spectrometer and to refine the calibration.

Microprobe analyses have been performed with a Cameca SX100 (Camparis, Univ. Paris 6). Classical analytical conditions were adopted for spot analyses [15 kV, 10 nA, wavelength-dispersive spectroscopy (WDS) mode], using Fe_2O_3 (Fe), $MnTiO_3$ (Mn, Ti), diopside (Mg, Si), CaF_2 (F), orthoclase (Al, K), anorthite (Ca) and albite (Na) as standards.

Raman spectroscopy on organic matter was done at Ecole Normale Supérieure of Paris, following the procedure described in Beyssac et al. (2002).

Appendix B. Supplementary data

Supplementary data to this article can be found online at doi:10.1016/j.lithos.2010.09.007.

References

Abers, G.A., van Keken, P.E., Kneller, E.A., Ferris, A., Stachnik, J.C., 2006. The thermal structure of subduction zones constrained by seismic imaging: implications for slab dehydration and wedge flow. Earth and Planetary Science Letters 241 (3–4), 387–397.

Agard, P., Yamato, P., Jolivet, L., Burov, E., 2009. Exhumation of oceanic blueschists and eclogites in subduction zones: timing and mechanisms. Earth-Science Reviews 92 (1–2), 53–79.

Alt, J., Honnorez, J., 1984. Alteration of the upper oceanic crust, DSDP site 417: mineralogy and chemistry. Contributions to Mineralogy and Petrology 87 (2), 149–169.

Amato, J.M., Johnson, C.M., Baumgartner, L.P., Beard, B.L., 1999. Rapid exhumation of the Zermatt–Saas ophiolite deduced from high-precision Sm–Nd and Rb–Sr geochronology. Earth and Planetary Science Letters 171 (3), 425–438.

Angiboust, S., Agard, P., Jolivet, L., Beyssac, O., 2009. The Zermatt–Saas ophiolite: the largest (60-km wide) and deepest (c. 70–80 km) continuous slice of oceanic lithosphere detached from a subduction zone? Terra Nova 21, 171–180.

Audet, P., Bostock, M.G., Christensen, N.I., Peacock, S.M., 2009. Seismic evidence for overpressured subducted oceanic crust and megathrust fault sealing. Nature 457 (7225), 76–78.

Auzende, A.L., Guillot, S., Devouard, B., Baronnet, A., 2006. Serpentinites in Alpine convergent setting: effects of metamorphic grade and deformation on microstructures. European Journal of Mineralogy 18, 21–33.

Baldelli, C., Dal Piaz, G.V., Lombardo, B., 1985. Ophiolite eclogites from Verres, Val d'Aosta, Western Alps, Italy. Chemical Geology 50, 87–98.

Ballevre, M., Merle, O., 1993. The Combin Fault — compressional reactivation of a Late Cretaceous–Early Tertiary Detachment Fault in the Western Alps. Schweizerische Mineralogische Und Petrographische Mitteilungen 73 (2), 205–227.

Ballevre, M., Pitra, P., Bohn, M., 2003. Lawsonite growth in the epidote blueschists from the Ile de Groix (Armorican Massif, France): a potential geobarometer. Journal of Metamorphic Geology 21 (7), 723–735.

Barnicoat, A.C., Fry, N., 1986. High-pressure metamorphism of the Zermatt-Saas ophiolite zone, Switzerland. Journal of the Geological Society 143 (4), 607–618.

Barnicoat, A.C., 1988. Zoned high-pressure assemblages in pillow lavas of the Zermatt–Saas ophiolite zone, Switzerland. Lithos 21 (3), 227–236.

Barnicoat, A.C., Bowtell, S.A., 1995. Sea-floor hydrothermal alteration in metabasites from high-pressure ophiolites of the Zermatt–Aosta area of the western Alps. Museo Regionale di Scienze Naturali di Torino, Bolletino 13, 191–220.

Barnicoat, A.C., Cartwright, I., 1995. Focused fluid flow during subduction: oxygen isotope data from high-pressure ophiolites of the western Alps. Earth and Planetary Science Letters 132 (1–4), 53–61.

Barnicoat, A.C., Fry, N., 1986. High-pressure metamorphism of the Zermatt–Saas ophiolite zone, Switzerland. Journal of the Geological Society 143, 607–618.

Barnicoat, A.C., Rex, D.C., Guise, P.G., Cliff, R.A., 1995. The timing of and nature of greenschist facies deformation and metamorphism in the upper Pennine Alps. Tectonics 14 (2), 279–293.

Bearth, P., 1959. Uber Eklogite, Glaucophanschiefer, und metamorphe Pillowlaven, Schweizerische Mineralogische und Petrographische Mitteilungen, pp. 267–286.

Bearth, P., 1964. Erläuterungen zu Blatt Randa, Geologischer Atlas der Schweiz Nr. 43, Schweiz. Geol. Kommission, Basel.

Bearth, P., 1966. Zur mineralfaziellen Stellung der Glaukophan-Gesteine der Westalpen. Schweizerische Mineralogische Und Petrographische Mitteilungen 46, 13–23.

Bearth, P., 1967. Die Ophiolithe der Zone von Zermatt–Saas Fee. MatÃ©riaux pour la Carte GÃ©ologique de la Suisse, Neue Folge(132).

Bearth, P., 1973. Gesteins- und Mineralparagenesen aus den Ophiolithen von Zermatt. Schweizerische Mineralogische Und Petrographische Mitteilungen 44, 15–26.

Bearth, P., Schwander, H., 1981. The post-Triassic sediments of the ophiolite zone Zermatt–Saas Fee and the associated manganese mineralizations. Eclogae Geologicae Helvetiae 198–205.

Bearth, P., Stern, W., 1971. Zum Chemismus der Eklogite und Glaukophanite von Zermatt. Schweizerische Mineralogische Und Petrographische Mitteilungen 51, 349–359.

Bearth, P. and Stern, W., 1979. Zur Geochemie von Metapillows der Region Zermatt-Saas. Schweizerische Mineralogische Und Petrographische Mitteilungen, 59.

Beltrando, M., Rubatto, D., Manatschal, G., 2010. From passive margins to orogens: the link between ocean–continent transition zones and (ultra)high-pressure metamorphism. Geology 38, 559–562.

Beyssac, O., Goffe, B., Chopin, C., Rouzaud, J.N., 2002. Raman spectra of carbonaceous material in metasediments: a new geothermometer. Journal of Metamorphic Geology 20 (9), 859–871.

Bostock, M.G., Hyndman, R.D., Rondenay, S., Peacock, S.M., 2002. An inverted continental Moho and serpentinization of the forearc mantle. Nature 417 (6888), 536–538.

Bucher, K., Grapes, R., 2009. The eclogite-facies Allalin Gabbro of the Zermatt–Saas ophiolite, Western Alps: a record of subduction zone hydration. Journal of Petrology 1405–1442.

Bucher, K., Fazis, Y., De Capitani, C., Grapes, R., 2005. Blueschists, eclogites, and decompression assemblages of the Zermatt–Saas ophiolite: high-pressure metamorphism of subducted Tethys lithosphere. American Mineralogist 90 (5–6), 821–835.

Cannat, M., Bideau, D., Bougault, H., 1992. Serpentinized peridotites and gabbros in the Mid-Atlantic Ridge axial valley at 15°37′N and 16°52′N. Earth and Planetary Science Letters 109 (1–2), 87–106.

Cannat, M., et al., 1995. Thin crust, ultramafic exposures, and rugged faulting patterns at the Mid-Atlantic Ridge. Geology 23 (1), 49–52.

Cartwright, I., Barnicoat, A.C., 1999. Stable isotope geochemistry of Alpine ophiolites: a window to ocean-floor hydrothermal alteration and constraints on fluid–rock interaction during high-pressure metamorphism. International Journal of Earth Sciences 88 (2), 219–235.

Cartwright, I., Barnicoat, A.C., 2002. Petrology, geochronology, and tectonics of shear zones in the Zermatt–Saas and Combin zones of the Western Alps. Journal of Metamorphic Geology 20 (2), 263–281.

Chinner, G.A., Dixon, J.E., 1973. Some high-pressure parageneses of Allalin Gabbro, Valais, Switzerland. Journal of Petrology 14 (2), 185–202.

Chopin, C., Monie, P., 1984. A unique magnesiochloritoid-bearing, high-pressure assemblage from the Monte-Rosa, Western Alps — petrologic and Ar-40–Ar-39 radiometric study. Contributions to Mineralogy and Petrology 87 (4), 388–398.

Chopin, C., Henry, C., Michard, A., 1991. Geology and petrology of the coesite-bearing terrain, Dora Maira Massif, Western Alps. European Journal of Mineralogy 3 (2), 263–291.

Chou, H.-C., Kuo, B.-Y., Chiao, L.-Y., Zhao, D., Hung, S.-H., 2009. Tomography of the westernmost Ryukyu subduction zone and the serpentinization of the fore-arc mantle. Journal of Geophysical Research. 114 (B12), B12301.

Clarke, G.L., Powell, R., Fitzherbert, J.A., 2006. The lawsonite paradox: a comparison of field evidence and mineral equilibria modelling. Journal of Metamorphic Geology 24, 715–725.

Connolly, J.A.D., 1990. Multivariable phase diagrams; an algorithm based on generalized thermodynamics. American Journal of Science 290 (6), 666–718.

Dal Piaz, G.V., Di Battistini, G., Kienast, J.-R., G, V., 1979. Manganiferous quartzitic schists of the Piemonte ophiolitic nappe in the Valsesia–Valtournanche area (Italian Western Alps). Memorie Sci Geol Padova 32.

Dal Piaz, G.V., Venturelli, G., Spadea, P., Di Battistini, G., 1981. Geochemical features of metabasalts and metagabbros from the Piemonte ophiolite nappe, Italian Western Alps, Neues Jahrb. Mineral. Abh. 142, 248–269.

Dal Piaz, G.V., et al., 2001. Tertiary age and paleostructural inferences of the eclogitic imprint in the Austroalpine outliers and Zermatt–Saas ophiolite, western Alps. International Journal of Earth Sciences 90 (3), 668–684.

Dal Piaz, G.V. et al., Carta geologica di Chatillon, Folio 091, 1/50, 000 scale map, Servizio geologico d'Italia, ISPRA, in press.
Dale, J., Powell, R., White, L., Elmer, F.L., Holland, T.J.B., 2005. A thermodynamic model of Ca–Na–amphiboles in Na_2O–CaO–FeO–MgO–Al_2O_3–SiO_2–H_2O–O for petrological calculations. Journal of Metamorphic Geology 23, 771–791.
Davis, P.B., Whitney, D.L., 2006. Petrogenesis of lawsonite and epidote eclogite and blueschist, Sivrihisar Massif, Turkey. Journal of Metamorphic Geology 24, 823–849.
Dercourt, J., Ricou, L.E., Vrielinck, B., 1993. Atlas Tethys Palaeo Environmental Maps. Gauthier-Villars, Paris.
Dick, H.J.B., et al., 2000. A long in situ section of the lower ocean crust: results of ODP Leg 176 drilling at the Southwest Indian Ridge. Earth and Planetary Science Letters 179 (1), 31–51.
Diener, J.F.A., Powell, R., White, R.W., Holland, T.J.B., 2007. A new thermodynamic model for clino- and orthoamphiboles in the system Na_2O–CaO–FeO–MgO–Al_2O_3–SiO_2–H_2O–O. Journal of Metamorphic Geology 25, 631–656.
Diener, J.F.A., Powell, R., 2010. Influence of ferric iron on the stability of mineral assemblages. Journal of Metamorphic Geology. doi:10.1111/j.1525-1314.2010.00880.x.
Droop, G.T.R., 1987. A general equation for estimating Fe^{3+} concentration in ferromagnesian silicates and oxides from microprobe analyses, using stoichiometric criteria. Mineralogy Magazine 51, 431–435.
Duchene, S., Lardeaux, J.M., Albarede, F., 1997. Exhumation of eclogites: insights from depth–time path analysis. Tectonophysics 280 (1–2), 125–140.
England, P.C., Holland, T.J.B., 1979. Archimedes and the Tauern eclogites — role of buoyancy in the preservation of exotic eclogite blocks. Earth and Planetary Science Letters 44 (2), 287–294.
Ernst, W.G., Dal Piaz, G.V., 1978. Mineral parageneses of eclogitic rocks and related mafic schists of Piemonte ophiolite nappe, Breuil-St-Jacques Area, Italian Western Alps. American Mineralogist 63 (7–8), 621–640.
Escartin, J., Hirth, G., Evans, B., 2001. Strength of slightly serpentinized peridotites: implications for the tectonics of oceanic lithosphere. Geology 29 (11), 1023–1026.
Federico, L., Crispini, L., Scambelluri, M., Capponi, G., 2007. Ophiolite melange zone records exhumation in a fossil subduction channel. Geology 35, 499–502.
Forneris, J.F., Holloway, J.R., 2004. Evolution of mineral compositions during eclogitization of subducting basaltic crust. American Mineralogist 89 (10), 1516–1524.
Fry, N., Barnicoat, A.C., 1987. The tectonic implications of high-pressure metamorphism in the western Alps. Journal of the Geological Society 144 (4), 653–659.
Fry, N. and Fyfe, W.S., 1971. On the significance of the eclogite facies in Alpine metamorphism. Verhandlungen der geologischen Bundesanstalt Wein, 2.
Garcia-Casco, A., Torres-Roldan, R.L., Millan, G., Monié, P., Schneider, J., 2002. Oscillatory zoning in eclogitic garnet and amphibole, Northern serpentinite mélange, Cuba: a record of tectonic instability during subduction? Journal of Metamorphic Geology 20, 581–598.
Gerya, T., Stöckhert, B., 2002. Exhumation rates of high pressure metamorphic rocks in subduction channels: the effect of Rheology. Geophysical Research Letters 29 (8), 1261.
Green, E.C.R., Holland, T.J.B., Powell, R., 2007. An order-disorder model for omphacitic pyroxenes in the system jadeite–diopside–hedenbergite–acmite, with applications to eclogite rocks. American Mineralogist 92, 1181–1189.
Groppo, C. and Castelli, D., in press. Prograde P–T evolution of a lawsonite eclogite from the Monviso metaophiolite (Western Alps): dehydration and redox reactions during subduction of oceanic FeTi-oxide gabbro. Journal of Petrology.
Groppo, C., Beltrando, M., Compagnoni, R., 2009. The PT path of the ultra-high pressure Lago Di Cignana and adjoining high-pressure meta-ophiolitic units: insights into the evolution of the subducting Tethyan slab. Journal of Metamorphic Geology 27, 207–231.
Guillot, S., Hattori, K.H., de Sigoyer, J., Nagler, T., Auzende, A.L., 2001. Evidence of hydration of the mantle wedge and its role in the exhumation of eclogites. Earth and Planetary Science Letters 193 (1–2), 115–127.
Guillot, S., Schwartz, S., Hattori, K., Auzende, A., Lardeaux, J., 2004. The Monviso ophiolitic Massif (Western Alps), a section through a serpentinite subduction channel. Evolution of the western Alps: insights from metamorphism, structural geology, tectonics and geochronology. The Virtual Explorer Paper 3.
Guillot, S., Hattori, K., Agard, P., Schwartz, S., Vidal, O., 2009. Exhumation processes in oceanic and continental subduction contexts: a review, subduction zone geodynamics. Frontiers in Earth Sciences. Springer, Berlin Heidelberg, pp. 175–205.
Hacker, B.R., Abers, G.A., 2004. Subduction factory 3: an Excel worksheet and macro for calculating the densities, seismic wave speeds, and H_2O contents of minerals and rocks at pressure and temperature. Geochemistry Geophysics Geosystems 5 (1), Q01005.
Hacker, B.R., Abers, G.A., Peacock, S.M., 2003a. Subduction factory 1. Theoretical mineralogy, densities, seismic wave speeds, and H_2O contents. Journal of Geophysical Research 108 (B1), 2029.
Hacker, B.R., Peacock, S.M., Abers, G.A., Holloway, S.D., 2003b. Subduction factory — 2. are intermediate-depth earthquakes in subducting slabs linked to metamorphic dehydration reactions? Journal of Geophysical Research-Solid Earth 108 (B1).
Harper, G.D., Bowman, J.R., Kuhns, R., 1988. A field, chemical, and stable isotope study of subseafloor metamorphism of the Josephine ophiolite, California–Oregon. Journal of Geophysical Research. 93 (B5), 4625–4656.
Heinrich, H., Althaud, E., 1988. Experimental determination of the reactions 4 lawsonite + 1 albite = 1 paragonite + 2 zoisite + 2 quartz + $6H_2O$ and 4 lawsonite + 1 jadeite = 1 paragonite + 2 zoisite + 1 quartz + $6H_2O$. Neues Jahrb. Mineral. Monatsh 11, 516–528.
Hilairet, N., Reynard, B., 2009. Stability and dynamics of serpentinite layer in subduction zone. Tectonophysics 465 (1–4), 24–29.
Hilairet, N., et al., 2007. High-pressure creep of serpentine, interseismic deformation, and initiation of subduction. Science 1910.
Holland, T.J.B., Powell, R., 1998. An internally consistent thermodynamic data set for phases of petrological interest. Journal of Metamorphic Geology 16 (3), 309–343.
Hyndman, R.D., Peacock, S.M., 2003. Serpentinization of the forearc mantle. Earth and Planetary Science Letters 212 (3–4), 417–432.
Ito, E., Harris, D.M., Anderson, A.T., 1983. Alteration of oceanic crust and geologic cycling of chlorine and water. Geochimica et Cosmochimica Acta 47 (9), 1613–1624.
Iwamori, H., 1998. Transportation of H_2O and melting in subduction zones. Earth and Planetary Science Letters 160 (1–2), 65–80.
Jambon, A., Zimmermann, J.L., 1990. Water in oceanic basalts: evidence for dehydration of recycled crust. Earth and Planetary Science Letters 101 (2–4), 323–331.
Konrad-Schmolke, M., O'Brien, P., De Capitani, C., Carswell, D., 2008. Garnet growth at high and ultra-high pressure conditions and the effect of element fractionation on mineral modes and composition. Lithos 103, 309–332.
Kretz, R., 1983. Symbols for rock-forming minerals. American Mineralogist 68, 277–279.
Lagabrielle, Y., Cannat, M., 1990. Alpine Jurassic ophiolites resemble the modern central Atlantic basement. Geology 18 (4), 319–322.
Lapen, T.J., et al., 2003. Burial rates during prograde metamorphism of an ultra-high-pressure terrane: an example from Lago di Cignana, western Alps, Italy. Earth and Planetary Science Letters 215 (1–2), 57–72.
Lapen, T., et al., 2007. Coupling of oceanic and continental crust during Eocene eclogite-facies metamorphism: evidence from the Monte Rosa nappe, western Alps. Contributions to Mineralogy and Petrology 153 (2), 139–157.
Le Bayon, B., Pitra, P., Ballevre, M., Bohn, M., 2006. Reconstructing PT paths during continental collision using multi-stage garnet (Gran Paradiso nappe, Western Alps). Journal of Metamorphic Geology 24, 477–496.
Leake, B.E., et al., 1997. Nomenclature of amphiboles: report of the subcommittee on amphiboles of the International Mineralogical Association, Commission on New Minerals and Mineral Names. American Mineralogist 82 (9–10), 1019–1037.
Lemoine, M., Tricart, P., Boillot, G., 1987. Ultramafic and gabbroic ocean floor of the Ligurian Tethys (Alps, Corsica, Apennines): in search of a genetic model. Geology 15, 622–625.
Li, X.P., Rahn, M., Bucher, K., 2004. Serpentinites of the Zermatt–Saas ophiolite complex and their texture evolution. Journal of Metamorphic Geology 22 (3), 159–177.
Liou, J.G., Hacker, B.R., Zhang, R.Y., 2000. Into the forbidden zone. Science 287, 1215–1216.
Marmo, B.A., Clarke, G.L., Powell, R., 2002. Fractionation of bulk rock composition due to porphyroblast growth: effects on eclogite facies mineral equilibria, Pam Peninsula, New Caledonia. Journal of Metamorphic Geology 20, 151–165.
Martin, S., Tartarotti, P., 1989. Polyphase HP Metamorphism in the Ophiolitic Glaucophanites of the Lower St. Marcel Valley (Aosta, Italy), Ofioliti, pp. 135–156.
Martin, S., Rebay, G., Kienast, J.R., Mevel, C., 2008. An eclogitized oceanic palaeo-hydrothermal field from the St Marcel valley (Italian Western Alps). Ofioliti 33 (1), 49–63.
Mével, C., 2003. Serpentinization of abyssal peridotites at mid-ocean ridges. Comptes Rendus Geosciences 335 (10–11), 825–852.
Michard, A., Chopin, C., Henry, C., 1993. Compression versus extension in the exhumation of the Dora-Maira coesite-bearing unit, Western Alps, Italy. Tectonophysics 221 (2), 173–193.
Miller, J.A., Cartwright, I., 2000. Distinguishing between seafloor alteration and fluid flow during subduction using stable isotope geochemistry: examples from Tethyan ophiolites in the Western Alps. Journal of Metamorphic Geology 18, 467–482.
Monié, P., Agard, P., 2009. Coeval blueschist exhumation along thousands of kilometers: implications for subduction channel processes. Geochemistry Geophysics Geosystems. 10 (7), Q07002.
Mottl, M.J., 1983. Metabasalts, axial hot springs, and the structure of hydrothermal systems at mid-ocean ridges. Geological Society of America Bulletin 94 (2), 161–180.
Oberhansli, R., 1982. The P–T history of some pillow lavas from Zermatt. Ofioliti 2, 431–436.
Oberhansli, R., 2004. Metamorphic Structure of the Alps. C.C.G.M, Paris.
Okamoto, K., Maruyama, S., 1999. The high-pressure synthesis of lawsonite in the MORB + H_2O system. American Mineralogist 84, 362–373.
Onken, O., et al., 2003. Seismic imaging of a convergent continental margin and plateau in the central Andes (Andean Continental Research Project 1996 (ANCORP'96)). Journal of Geophysical Research 108 (B7), 2328.
Peacock, S.A., 1990. Fluid processes in subduction zones. Science 248 (4953), 329–337.
Peacock, S.M., 1993. The importance of blueschist–eclogite dehydration reactions in subducting oceanic crust. Geological Society of America Bulletin 105 (5), 684–694.
Peacock, S.M., Hyndman, R.D., 1999. Hydrous minerals in the mantle wedge and the maximum depth of subduction thrust earthquakes. Geophysical Research Letters 26 (16), 2517–2520.
Pfeifer, H.R., Colombi, A., Ganguin, J., 1989. Zermatt–Saas and Antrona Zone: a petrographic and geochemical comparison of polyphase metamorphic ophiolites of the West-Central Alps. Schweizerische Mineralogische und Petrographische Mitteilungen 69 (2), 216–236.
Platt, J.P., 1993. Exhumation of high-pressure rocks — a review of concepts and processes. Terra Nova 5 (2), 119–133.
Pognante, U., 1985. Coronitic reaction and ductile shear zones in eclogitized ophiolite metagabbro, Western Alps, North Italy. Chemical Geology 50, 99–109.
Pognante, U., 1989. Tectonic implications of lawsonite formation in the Sesia zone (Western Alps). Tectonophysics 162 (3–4), 219–227.
Poli, S., Schmidt, M.W., 1995. H_2O transport and release in subduction zones: experimental constraints on basaltic and andesitic systems. Journal of Geophysical Research 100 (B11), 22299–22314.
Raimbourg, H., Jolivet, L., Leroy, Y., 2007. Consequences of progressive eclogitization on crustal exhumation, a mechanical study. Geophysical Journal International 168 (1), 379–401.

Ranero, C.R., Phipps Morgan, J., McIntosh, K., Reichert, C., 2003. Bending-related faulting and mantle serpentinization at the Middle America trench. Nature 425 (6956), 367–373.
Rebay, G., Powell, R., Diener, J.F.A., 2010. Calculated phase equilibria for a MORB composition in a P–T range, 450–650 °C and 18–28 kbar: the stability of eclogites. Journal of Metamorphic Geology 28 (6), 635–645.
Reinecke, T., 1991. Very-high-pressure metamorphism and uplift of coesite-bearing metasediments from the Zermatt–Saas zone, Western Alps. European Journal of Mineralogy 3 (1), 7–17.
Reinecke, T., 1998. Prograde high- to ultrahigh-pressure metamorphism and exhumation of oceanic sediments at Lago di Cignana, Zermatt–Saas Zone, western Alps. Lithos 42 (3–4), 147–189.
Rogers, G., Dragert, H., 2003. Episodic tremor and slip on the Cascadia subduction zone: the chatter of silent slip. Science 300 (5627), 1942–1943.
Rubatto, D., Hermann, J., 2001. Exhumation as fast as subduction? Geology 29 (1), 3–6.
Rubatto, D., Gebauer, D., Fanning, M., 1998. Jurassic formation and Eocene subduction of the Zermatt–Saas–Fee ophiolites: implications for the geodynamic evolution of the Central and Western Alps. Contributions to Mineralogy and Petrology 132 (3), 269–287.
Scambelluri, M., Muntener, O., Hermann, J., Piccardo, G.B., Trommsdorff, V., 1995. Subduction of water into the mantle: history of an Alpine peridotite. Geology 23 (5), 459–462.
Schmidt, M.W., Poli, S., 1998. Experimentally based water budgets for dehydrating slabs and consequences for arc magma generation. Earth and Planetary Science Letters 163 (1–4), 361–379.
Schwartz, S., Lardeaux, J.M., Guillot, S., Tricart, P., 2000. Diversité du métamorphisme éclogitique dans le massif ophiolitique du Monviso (Alpes Occidentales, Italie). Geodinamica Acta 13, 169–188.
Schwartz, S., Allemand, P., Guillot, S., 2001. Numerical model of the effect of serpentinites on the exhumation of eclogitic rocks: insights from the Monviso ophiolitic massif (Western Alps). Tectonophysics 342 (1–2), 193–206.
Seifert, K., Brunotte, D., 1996. Geochemistry of serpentinized mantle peridotite from Site 897 in the Iberia Abyssal Plain. Proceedings of the Ocean Drilling Program Scientific Results 149, 801.
Seno, T., 2005. Variation of downdip limit of the seismogenic zone near the Japanese islands: implications for the serpentinization mechanism of the forearc mantle wedge. Earth and Planetary Science Letters 231 (3–4), 249–262.
Seyfried, W.E., Mottl, M.J., BlSchoff, J.L., 1978. Seawater/basalt ratio effects on the chemistry and mineralogy of spilites from the ocean floor. Nature 275 (5677), 211–213.
Shreve, R.L., Cloos, M., 1986. Dynamics of sediment subduction, melange formation, and prism accretion. Journal of Geophysical Research-Solid Earth and Planets 91 (B10), 229–245.
Singh, S.C., et al., 2008. Seismic evidence for broken oceanic crust in the 2004 Sumatra earthquake epicentral region. Nature Geosciences 1 (11), 777–781.
Staudigel, H., Plank, T., White, B., Schmincke, H.U., 1996. Geochemical Fluxes during Seafloor Alteration of the Basaltic Upper Oceanic Crust: DSDP Sites 417 and 418. American Geophysical Union, Washington, DC, USA. 391 pp.
Tartarotti, P., Martin, S., Polino, R., 1986. Geological data about the ophiolitic sequences in the St. Marcel valley (Aosta Valley). Ofioliti 11, 343–346.
Tartarotti, P., Benciolini, L., Monopoli, B., 1998. Brecce serpentinitiche nel massiccio ultrabasico del Monte Avic (Falda ofiolitica piemontese): possilibi evidenze di erosione sottomarina. Atti Ticinensi Sci Terra 7, 73–86.
Tsujimori, T., Sisson, V.B., Liou, J.G., Harlow, G.E., Sorensen, S.S., 2006. Very-low-temperature record of the subduction process: a review of worldwide lawsonite eclogites. Lithos 92 (3–4), 609–624.
Ulmer, P., Trommsdorff, V., 1995. Serpentine stability to mantle depths and subduction-related magmatism. Science 268 (5212), 858–861.
Van der Klauw, S.N.G.C., Reinecke, T., Stöckhert, B., 1997. Exhumation of ultrahigh-pressure metamorphic oceanic crust from Lago di Cignana, Piemontese zone, western Alps: the structural record in metabasites. Lithos 41, 79–102.
Warren, C., Waters, D., 2006. Oxidized eclogites and garnet-blueschists from Oman: P–T path modelling in the NCFMASHO system. Journal of Metamorphic Geology 24, 783–802.
Wei, C.J., Song, S.G., 2008. Chloritoid-glaucophane schist in the north Qilian orogen, NW China: phase equilibria and PT path from garnet zonation. Journal of Metamorphic Geology 26, 301–316.
Wei, C.J., Powell, R., Zhang, L.F., 2003. Eclogites from the south Tianshan, NW China: petrological characteristic and calculated mineral equilibria in the Na_2O–CaO–FeO–MgO–Al_2O_3–SiO_2–H_2O system. Journal of Metamorphic Geology 21 (2), 163–179.
Wheeler, J., Buttler, R.W.H., 1993. Evidence for extension in the western Alpine orogen: the contact between the oceanic Piemonte and overlying continental units. Earth and Planetary Science Letters 117, 457–474.
Wheeler, J., Reddy, S.M., Cliff, R.A., 2001. Kinematic linkage between internal zone extension and shortening in more external units in the NW Alps. Journal of the Geological Society 158 (3), 439–443.
White, R.W., Powell, R., Holland, T.J.B., Worley, B.A., 2000. The effect of TiO_2 and Fe_2O_3 on metapelitic assemblages at greenschist and amphibolite facies conditions: mineral equilibria calculations in the system K_2O–FeO–MgO–Al_2O_3–SiO_2–H_2O–TiO_2–Fe_2O_3. Journal of Metamorphic Geology 18, 497–511.
White, R.W., Powell, R., Phillips, G.N., 2003. A mineral equilibria study of the hydrothermal alteration in mafic greenschist facies rocks at Kalgoorlie, Western Australia. Journal of Metamorphic Geology 21, 455–468.
Widmer, T., 1996. Entwasserung ozeanisch alterierter Basalte in Subduktionszonen (Zone von Zermatt–Saas Fee). Dissertation Nr 11609, Zurich.
Widmer, T., Ganguin, J., Thompson, A.B., 2000. Ocean floor hydrothermal veins in eclogite facies rocks of the Zermatt–Saas zone, Switzerland. Schweizerische Mineralogische Und Petrographische Mitteilungen 80, 63–73.
Xia, S., Zhao, D., Qiu, X., 2008. Tomographic evidence for the subducting oceanic crust and forearc mantle serpentinization under Kyushu, Japan. Tectonophysics 449 (1–4), 85–96.